Modelling Distillation with Non-Equilibrium Thermodynamics

Mari Voldsund

NTNU
Spring 2009

Declaration

I declare that the work presented in this thesis has been carried out independently and in agreement with "Reglement for sivilarkitekt- og sivilingeniøreksamen".

Trondheim, July 1st 2009

Mari Voldsund

Preface

This thesis is submitted to the Department of Chemistry, Faculty of Natural Sciences and Technology, Norwegian University of Science and Technology (NTNU) in partial fulfillment of the Master of Technology degree. It concludes a five year education programme in Physical Chemistry at NTNU.

The thesis work was limited to 20 weeks and has been carried out from January to June 2009 under the supervision of Signe Kjelstrup.

Acknowledgements

First I would like to thank my supervisor, Signe Kjelstrup, for including me in her research group on non-equilibrium thermodynamics, and for giving me the chance to work on this project. Her guidance and valuable advices are highly appreciated, also her effectiveness and her inspiring personality. A thank is also given to Dick Bedeaux and Kirill Glavatskiy for help with understanding the theory of non-equilibrium thermodynamics. Audun Røsjorde is thanked for help and information about real distillation columns. I would like to thank Leen van der Ham and Robert Bock for helpful discussions about theory, method and calculations. A big thank is given to Einar Ryeng for help with all kinds of computer related problems and for help with language. Sondre Schnell Kvalvåg, Magnus Ringholm, Ingrid Aaen, Anders Lervik and Odne Stokke Burheim are thanked for moral support and for fruitful discussions about small and big problems concerning the project.

Finally I would like to thank absolutely everyone at physical chemistry for making my time as a physical chemistry student a really enjoyable time. I have really appreciated their company, and the time spent with them has been both educative and fun.

Summary

A method for calculating fluxes and temperature and chemical potential profiles over interfaces using an approach called *the integrated interface approach* is established for systems with known properties of bulk phases for vapor and liquid and a system in steady state. In the integrated interface approach flux equations are derived in a systematic manner using non-equilibrium thermodynamics including all possible coupling effects and opening for the possibility of non-equilibrium over the interface. The system where the transport between the two phase bulks takes place is treated as three subsystems; the vapor diffusion film, the interface and the liquid diffusion film. Resistivities and local driving forces are assumed constant within each of these subsystems.

A de-ethanizer distillation column is modelled using ChemSep, a commercially available software where an approach developed by Taylor and Krishna is used. In their approach equilibrium over the interface is assumed, and coupling between heat and mass transport is neglected. It is shown that when these assumptions are taken in the integrated interface approach will the two approaches be equivalent, except for the mass and heat transfer coefficients used.

New fluxes and temperature and chemical potential profiles are calculated using the integrated interface approach. The impact of the choice of diffusion film thicknesses and Soret coefficients is examined. The calculated fluxes and profiles are compared with the fluxes and profiles calculated by ChemSep. The importance of including non-equilibrium over the interface and coupling of heat and mass transport is examined by neglecting these effects and comparing the results with calculations where all these effects are included.

Both the choice of film thickness and Soret coefficients had a high impact on the system. The dependecy on the film thicknesses was especially high, at the same time as this value is related to a high level of uncertainity.

The fluxes calculated by ChemSep deviate widely from the fluxes calculated using the integrated interface approach, also when the same assumptions concerning interface and coupling are used. This deviation is then due to the different coefficients used. The impact of including non-equilibrium over the interface and coupling between heat and mass transport is shown to be small for the distillation column considered here. Both neglecting the interface resistance and multiplying the interface resistance with 10 change the fluxes with less than 0.5 %. Neglecting the coupling of heat and mass transport changes the fluxes with less than 2 %. The impact of these effects can be higher for other distillation prosesses.

Contents

Chapter 1

Introduction

Distillation is a separation method where chemical components are separated based on their different volatilities. Distillation columns are important process equipment that are widely used in the industry. The process is the most common separation method, and it consumes large amounts of energy. In 1991 it accounted for 11 % of the industrial energy demand in the United States [7]. Good models can help to design better and more energy efficient columns, and through this save the environment.

The classical distillation model has been an equilibrium model. In such models equilibrium is assumed between the vapor and liquid stream leaving each distillation tray. In reality such an equilibrium is not reached. The Murphree efficiency was introduced to account for this irreversibility [9]. This efficiency measures to which degree equilibrium is reached. However, this efficiency provides no physical explanation for why equilibrium is not reached.

During the last 30 years also non-equilibrium models have been introduced. They seek to model the distillation processes more accurate by assuming equilibrium only at the interface, and then include the transport of heat and mass that take place in the liquid and the vapor phases. Taylor and Krishna have played central roles in the development of such models, and they describe their research in the book "Multicomponent Mass Transfer" [17]. They propose to use mass transfer coefficients from correlations that apply to the type of equipment. ChemSep [1] is a commercially available software where Taylor and Krishna's approach is used, and it is developed by among others Taylor.

By using irreversible thermodynamics, transport equations for distillation can be derived in a systematic way with all possible coupling effects included. The approach of Taylor and Krishna is based on irreversible thermodynamics, but they neglect the coupling of heat and mass transport. Kjelstrup and de Koeijer have developed a more general formulation called the interface integrated approach [11]. This approach includes all coupling effects. It also includes the possibilty for not having equilibrium across the interface by treating the interface as a separate phase where only local equilibrium is assumed.

This project aims to calculate fluxes in distillation columns using the integrated interface approach. A closer look is taken at the differences between this approach and Taylor and Krishna's approach. The importance of including effects from non-equilibrium over the interface and from coupling between heat and mass is investigated for transport equations for use in non-equilibrium distillation models.

A de-ethanizer column is modelled using ChemSep, and new fluxes are calculated for this

column. The fluxes are calculated both with and without including the effects mentioned above, and the differences are investigated. The calculated fluxes are also compared to the fluxes calculated by ChemSep, to see the differences between the two approaches.

The project is a part of an overall effort at Department of Chemistry to find applications for the theory of non-equilibrium thermodynamics. A long term goal is to make an accurate non-equilibrium distillation model using the integrated interface approach.

The remainder of this thesis is outlined as follows: First the relevant theory is presented in chapter 2. The concept of distillation is explained and a general introduction to non-equilibrium thermodynamics and to different descriptions of the interface is given. Taylor and Krishna's approach to non-equilibrium distillation and the integrated interface approach is presented. A comparison between the theory of the to approaches is given. Then the method used to do the calculations are described in chapter 3. The results are presented and discussed in chapter 4, and eventually in this chapter are suggestions for further work described. A conclusion is given in chapter 5.

Chapter 2

Theory

2.1 Distillation

A distillation process is a process in which the varying volatility of chemical components are used to separate them. Because of the varying volatility, the distribution of the components in the vapor and the liquid phase is different. If a part of a mixture is evaporated, the vapor phase will be richer on the more volatile component than the liquid phase. The vapor phase can be condensed, and the process can be repeated to give an even purer vapor phase. Distillation is done industrially in distillation columns where evaporations and condensations are done in several stages. The vapor of each stage will continually flow up and mix with the contents of the stage above, and the liquid will flow down to the step below. There are two main designs of distillation columns; tray columns and packed columns. Only tray columns are considered in this project. In tray columns, each column stage consists of a tray in which liquid and vapor are brought into contact.

2.2 Non-equilibrium thermodynamics

In this section a short presentation on non-equilibrium thermodynamics, also called irreversible thermodynamics, will be given following Førland, Førland and Kjelstrup [5] and Kjelstrup and Bedeaux [10].

Non-equilibrium thermodynamics can be used to describe systems which are not in global equilibrium. The theory describes interacting transport processes in a systematic way, using fluxes and forces obtained from the entropy production. Coupling between different types of transport in the same system is included. The description in this section will be limited to systems with only heat and mass transport.

The local entropy production of a system, σ, can be written as the product sum of fluxes, J_i, and driving forces, X_i. The second law of thermodynamics gives:

$$\sigma = \sum_i J_i X_i \geq 0 \tag{2.1}$$

The total entropy production is the integral of this over the volume. A basic assumption in non-equilibrium thermodynamics is that each of these fluxes is given by linear combinations of

the driving forces:

$$J_i = \sum_j L_{ij} X_j \tag{2.2}$$

where the L's express conductivity. The theory is limited to systems with microscopic reversibility. For such a system, the reciprocal relation has been proven:

$$L_{ij} = L_{ji} \tag{2.3}$$

The flux equations, equation 2.2, can alternatively be written as forces that are linear combinations of fluxes:

$$X_i = \sum_j R_{ij} J_j \tag{2.4}$$

where the R's express resistivity, and we have the relation:

$$R \times L = I \tag{2.5}$$

where R and L are $n \times n$ matrices with the resistivities and conductivities of the system and I is the identity matrix. Now the reciprocal relation is expressed as:

$$R_{ij} = R_{ji} \tag{2.6}$$

It can be shown that as a consequence of the second law of thermodynamics must all pairs of coefficients obey the following boundary condition:

$$R_{ii} R_{jj} - R_{ij} R_{ji} \geq 0 \tag{2.7}$$

2.3 Description of interface

An interface is the thin layer between two different homogeneous phases. It is often looked upon as a two dimensional surface that not has any volume, nor any other extensive variables. It is often assumed to be equilibrium over the interface, so that temperature and chemical potential is continous through this surface. This means that the temperature and chemical potential at each side of the surface has to be the same. A shematic overview of a temperature profile for a system out of equilibrium, but with equilibrium over the interface is given in figure 2.1. In Taylor and Krishna's approach to non-equilibrium distillation, the interface between vapor and liquid is treated like this.

If a higher preciseness is needed, the description above is not good enough. The interface layer has a thickness, even though it is small, and thus also a volume and other extensive variables. Already in 1874 Gibbs described how these layers can have special profiles for intensive variables [15]. He constructed a thermodynamic description of equilibrium surfaces in terms of excess densities and treated the surface as an autonomous thermodynamic system. The description implies for instance that the surface has its own temperature. Kjelstrup and Bedeaux [10] show how Gibbs description of interfaces in systems with global equilibrium can be extended to systems that are out of equilibrium, also over the interface. Then local equilibrium has to be assumed through the whole system. Now temperatures and chemical potentials do not have to be the same on each side of the interface. The property of the interface that is of interest for this project is the entropy production, to be able to calculate the fluxes and the forces of the system. This is treated more in detail in section 2.5, and after some assumptions we shall see that only the properties on each side on the interface are of importance. A shematic overview of a temperature profile for such a system is given in figure 2.2, where the profile inside the surface is left out since it is not needed in this project.

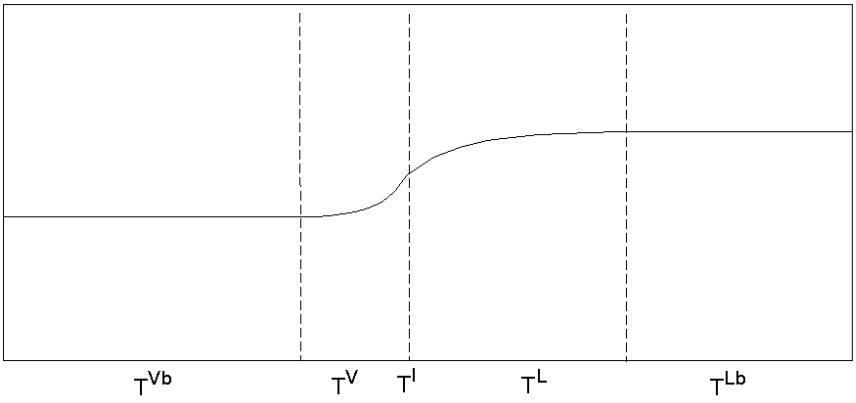

Figure 2.1: Shematic overview of temperature profile in a two phase system with equilibrium across the interface.

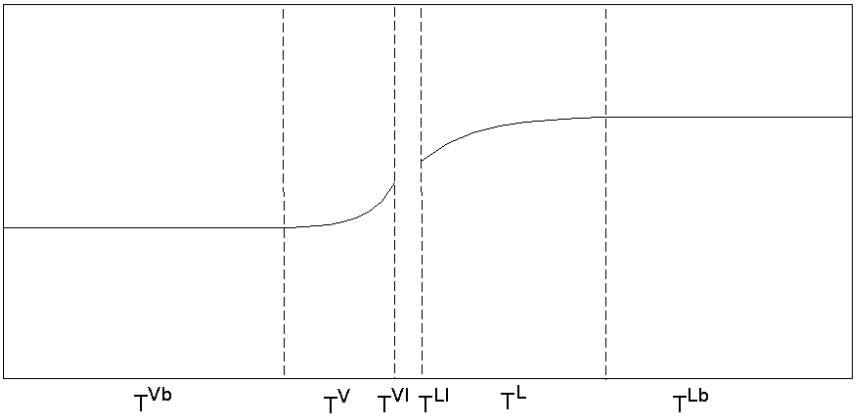

Figure 2.2: Shematic overview of temperature profile in a two phase system where the interface is treated as a separate thermodynamic system where only local equilibrium is assumed.

2.4 Modelling non-equilibrium distillation

The following section is based on Taylor and Krishna's [17] discussion of nonequilibrium stage models on multicomponent distillation.

A non-equilibrium model will include material balances, energy balances, equilibrium relations, summation equations and mass and energy transfer models. The mass and energy balances are written for each phase in the considered stage. The balances are linked together, as all components leaving one phase have to enter the other phase. Equilibrium relations are used to relate compositions of either side of the phase interface. These realtions are dependent on temperature and compostion at the interface. Transport equations describe the transfer of mass and energy inside the phases.

Throughout this section, all main equations are written on a form with zero on the left hand side, as they are intended to be solved numerically, and each such equation is given a letter in the font sansserif. L and V are molar liquid and gas streams, respectively. x and y are molar

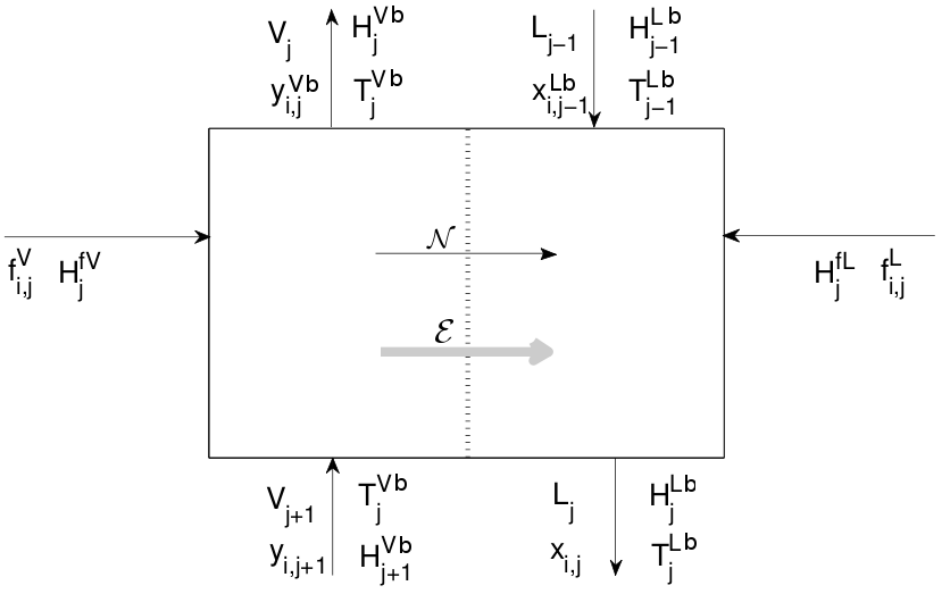

Figure 2.3: Shematic illustration of flows of mass and energy in tray j in a distillation column. The dashed line represents the interface. The thin, black arrows represent mass transfer, and the thick, grey arrows represent energy transfer. $\mathcal{N}$ refers to interface mass transport while $\mathcal{E}$ refers to interface energy transport.

fractions of the liquid and gas phases. H is molar enthalpy, T is temperature and Q is heat stream. f is molar feed. In this section subscript i refers to component i, and subscript j refers to stage j. Superscript V refers to the vapor diffusion film and L refers to the liquid diffusion film, superscript I refers to interface, fV refers to vapor feed, fL refers to liquid feed, Vb refers to the vapor bulk and Lb refers to the liquid bulk.

A shematic illustration of a distillation tray is given in figure 2.3.

2.4.1 Mass balances

On the principle of conservation of mass, balance equations of both phases can be written for each stage. There is no accumulation of mass in the system.

The component material balance for the two phases can be written as follows:

$$\begin{aligned} \mathsf{M}_{ij}^{V} &\equiv V_j y_{ij}^{Vb} - V_{j+1} y_{i,j+1}^{Vb} - f_{ij}^{V} + \mathcal{N}_{ij}^{V} \\ &= 0 \end{aligned} \tag{2.8}$$

$$\begin{aligned} \mathsf{M}_{ij}^{L} &\equiv L_j x_{ij}^{Lb} - L_{j-1} x_{i,j-1}^{Lb} - f_{ij}^{L} - \mathcal{N}_{ij}^{L} \\ &= 0 \end{aligned} \tag{2.9}$$

where $\mathcal{N}$ refers to the interphase transport, and transport from the vapor to the liquid phase is defined positive. No mass accumulates at the interphase, implying the following equation:

$$\mathsf{M}_{ij}^{I} \equiv \mathcal{N}_{ij}^{V} - \mathcal{N}_{ij}^{L} = 0 \tag{2.10}$$

By summing equation 2.8 and equation 2.9 over the components, the total material balances for stage j are obtained:

$$\mathsf{M}_{t_j}^V \equiv V_j - V_{j+1} - F_j^V + \mathcal{N}_{t_j}^V = 0 \tag{2.11}$$

$$\mathsf{M}_{t_j}^L \equiv L_j - L_{j-1} - F_j^L - \mathcal{N}_{t_j}^L = 0 \tag{2.12}$$

where the subscript t means total, $F_j = \sum_{i=1}^{c} f_{ij}$ and $\mathcal{N}_{tj} = \sum_{i=1}^{c} \mathcal{N}_{ij}$. The interphase mass transport is described in section 2.4.3.

2.4.2 Energy balances

When assuming no heat leakage from the column, the conservation law yield the following balance for energy in the vapor phase and gas phase respectively:

$$\mathsf{E}_{ij}^V \equiv V_j H_j^{Vb} - V_{j+1} H_{j+1}^{Vb} - F_j^V H_j^{fV} + Q_j^V - \mathcal{E}_j^V = 0 \tag{2.13}$$

$$\mathsf{E}_{ij}^L \equiv L_j H_j^{Lb} - L_{j-1} H_{j-1}^{Lb} - F_j^L H_j^{fL} + Q_j^L - \mathcal{E}_j^L = 0 \tag{2.14}$$

where H are molar enthalpies, Q is heat added or withdrawed from the tray, and $\mathcal{E}$ represents the energy loss or gain due to interphase transfer.

As there is no energy accumulation at the interface, an energy balance yields:

$$\mathsf{E}_{ij}^I \equiv \mathcal{E}_j^V - \mathcal{E}_j^L = 0 \tag{2.15}$$

2.4.3 Taylor and Krishna's transport equations

The mass transfer rates in the vapor and liquid diffusion films have to be modelled. The fluxes inside each bulk phase, relative to a stationary interface, can be given by:

$$J_i^{V,TK} = J_{i,am}^{V,TK} + J_t^{V,TK} y_i^{Vb} \tag{2.16}$$

$$J_i^{L,TK} = J_{i,am}^{L,TK} + J_t^{L,TK} x_i^{Lb} \tag{2.17}$$

where the superscript TK indicates that these are the transport equations used by Taylor and Krishna. am indicate that the flux is relative to the average molar velocity. J_t is the mixture molar flux.

Ideally mixed bulk phases with diffusion films along the interface are assumed. Taylor and Krishna estimate the molar diffusion fluxes with the following equations:

$$(J_{am}^{V,TK}) = c^V [k^V](y^{Vb} - y^I) \tag{2.18}$$

$$(J_{am}^{L,TK}) = c^L [k^L](x^I - x^{Lb}) \tag{2.19}$$

where $[k^V]$ and $[k^L]$ are matrices with mass transfer coefficients.

$$[k^P] = [R^P]^{-1}[\Gamma] \tag{2.20}$$

where the superscript P refers to an arbitrary phase, $[R]$ is a matrix with mass transfer resistances and $[\Gamma]$ is a matrix of thermodynamic factors. The matrix of thermodynamic factors appears bacause the fundamental driving force for mass transfer is the chemical potential gradient, and not the mole fraction gradient.

The resistances are calculated from the following formulae:

$$R_{ii}^P = \frac{z_i}{k_{ic}^P} + \sum_{k=1,k\neq i}^{c} \frac{z_k}{k_{ik}^P} \tag{2.21}$$

$$R_{ij}^P = -z_i \left(\frac{1}{k_{ij}^P} - \frac{1}{k_{ic}^P} \right) \tag{2.22}$$

where z is the mole fraction of the phase in question and the k's are binary mass transfer coefficients computed from empirical models. c is te number of components in the system.

The thermodynamic factor matrix Γ is defined by:

$$\Gamma_{ij}^P = \delta_{ij} + z_i \left(\frac{\partial \ln \phi_i^P}{\partial z_j} \right)_{T,P,z_k,k\neq j=1,\ldots,c-1} \tag{2.23}$$

where δ_{ij} is the Kronecker delta and ϕ is the fugacity coefficient. When the mixture is ideal, the thermodynamic factor matrix is an identity matrix.

By combining the equations 2.16 - 2.19 and multiplying with the interfacial area, a_j, the total mass transfer rates for the two phase bulks in each stage are obtained:

$$\mathcal{N}_{ij}^V = c^V [k_j^V] a_j (y_{ij}^{Vb} - y_{ij}^I) + \mathcal{N}_{t_j}^V y_{ij}^{Vb} \tag{2.24}$$

$$\mathcal{N}_{ij}^L = c^L [k_j^L] a_j (x_{ij}^I - x_{ij}^{Lb}) + \mathcal{N}_{t_j}^L x_{ij}^{Lb} \tag{2.25}$$

where $\mathcal{N}_{t_j} = a_j J_{t_j}^{TK}$ is the total mass trasfer rate on stage j and a_j is the net interfacial area of stage j. The interfacial area is dependent on equipment and operating conditions, and can be found from empirical models.

Since the system described is steady state, there can not be any accumulation at the interface, so there are only one set of independent mass transfer rates, and $\mathcal{N}_{ij} = \mathcal{N}_{ij}^V = \mathcal{N}_{ij}^L$ can be substituted into equation 2.8, 2.9, 2.11 and 2.12. By combining the mass transfer rate equations and the interface material balances the following relations occur:

$$\mathsf{R}_{ij}^V \equiv \mathcal{N}_{ij} - \mathcal{N}_{ij}^V = 0 \tag{2.26}$$

$$\mathsf{R}_{ij}^L \equiv \mathcal{N}_{ij} - \mathcal{N}_{ij}^L = 0 \tag{2.27}$$

The heat flux for each phase can be written as:

$$J_q^{V,TK} = h_j^V (T_j^{Vb} - T_j^I) + \sum_{i=1}^{c} J_{ij}^{V,TK} \overline{H}_{ij}^{Vb} \tag{2.28}$$

$$J_q^{L,TK} = h_j^L (T_j^I - T_j^{Lb}) + \sum_{i=1}^{c} J_{ij}^{L,TK} \overline{H}_{ij}^{Lb} \tag{2.29}$$

where h_j is the heat transfer coefficient, and $\overline{H}_{ij}$ is the partial molar enthalpy of component i for stage j.

The energy transfer rates are obtained by multiplying the fluxes with the interfacial area, a_j:

$$\mathcal{E}_j^V = h_j^V a_j (T_j^{Vb} - T_j^I) + \sum_{i=1}^{c} \mathcal{N}_{ij} \overline{H}_{ij}^{Vb} \tag{2.30}$$

$$\mathcal{E}_j^L = h_j^L a_j (T_j^I - T_j^{Lb}) + \sum_{i=1}^{c} \mathcal{N}_{ij} \overline{H}_{ij}^{Lb} \tag{2.31}$$

2.4.4 The interface model

At the interface, there is assumed to exist phase equilibrium, as in figure 2.1. At face equilibrium the ratio between the vapor and liquid mole fraction of each component is called the K-value of this component:

$$K_{ij} = \frac{y_{ij}^I}{x_{ij}^I} \tag{2.32}$$

where K is the K-value. This value is dependent on temperature and composition at the interface. Rewriting this equation gives:

$$\mathsf{Q}_{ij}^I = K_{ij} x_{ij}^I - y_{ij}^I = 0 \tag{2.33}$$

Furthermore, the mole fractions at the interface have to sum to unity:

$$\mathsf{S}_j^{VI} = \sum_{i=1}^{c} y_{ij}^I - 1 = 0 \tag{2.34}$$

$$\mathsf{S}_j^{LI} = \sum_{i=1}^{c} x_{ij}^I - 1 = 0 \tag{2.35}$$

2.4.5 Hydraulic equations

The pressure drop over the column depends on the design and the operating conditions. The pressure of each tray is dependent on the tray above, and this can be expressed as follows:

$$\mathsf{P}_j \equiv P_j - P_{j-1} - (\Delta P_{j-1}) = 0 \tag{2.36}$$

where P_j is the pressure of stage j, and ΔP_{j-1} is the pressure drop from stage $j-1$ to stage j. If the column has a condenser, the pressure has to be specified, and the condenser is numbered as stage 1. The pressure of the top tray also has to be specified, and this is numbered as stage 2.

$$\mathsf{P}_1 \equiv P_c - P_1 = 0 \tag{2.37}$$

$$\mathsf{P}_2 \equiv P_s - P_2 = 0 \tag{2.38}$$

where P_c is the pressure of the condenser, and P_s is the specified pressure of the top tray.

2.4.6 ChemSep

Taylor has used the theory presented here to develop the non-equilibrium distillation model program ChemSep [1]. The approach has been tested for various systems, compared with real systems and found to give good results, see Taylor and Krishna [17], Krishnamurthy and Taylor [14] and the ChemSep Book [12].

2.5 The integrated interface approach

In this section diffusive transport equations for a heterogenous system with two components and only heat and mass transport are derived using non-equilibrium thermodynamics including non-equilibrium over the interface. The approach used by Kjelstrup and de Koeijer [11] is followed, but in this document the fluxes are defined positive when directed from vapor to liquid. The approach is called the integrated interface approach. The system consists of a bulk phase with vapor, a diffusion layer in the vapor, an interface, a diffusion layer in the liquid and bulk phase with liquid, as shown in figure 2.2. The bulk phases are assumed to be uniform. The system is in a stationary state, so the mass fluxes and the total heat flux is constant throughout the system. The measurable heat flux, however, is not constant due to changes in molar enthalpies at the phase transitions. All fluxes and forces are assumed to be perpendicular to the interface, so for the derivation of these equations, the system can be considered one dimensional.

The total entropy production rate of the system is then:

$$\frac{dS^{irr}}{dt} = \frac{dS^{irr,V}}{dt} + \frac{dS^{irr,I}}{dt} + \frac{dS^{irr,L}}{dt} \tag{2.39}$$

where $\frac{dS^{irr}}{dt}$ is total entropy production, and here the superscript V refers to the vapor diffusion film, I refers to the interface and L refers to the liquid diffusion film.

2.5.1 Interface

For an interface with a binary mixture, the entropy production along a one-dimensional part across the whole interface can be written:

$$\frac{dS^{irr,I}}{dt} = J_q'^V X_q'^I + J_1 X_1^I + J_2 X_2^I \tag{2.40}$$

$J_q'^V$ is the measurable heat flux in the vapor, and J_1 and J_2 are the fluxes of component 1 and 2. A derivation of this expression is given in appendix A.1.1 where the following driving forces are obtained:

$$X_q'^I = \Delta_{VI,LI}\left(\frac{1}{T}\right) \tag{2.41}$$

$$X_1^I = -\frac{1}{T^{LI}}\Delta_{VI,LI}\mu_{1,T}(T^{LI}) \tag{2.42}$$

$$X_2^I = -\frac{1}{T^{LI}}\Delta_{VI,LI}\mu_{2,T}(T^{LI}) \tag{2.43}$$

Each driving force can be written as a sum of products of resistivities and fluxes:

$$X_q'^I = r^I_{qq} J_q'^V + r^I_{q1} J_1 + r^I_{q2} J_2 \tag{2.44}$$
$$X_1^I = r^I_{1q} J_q'^V + r^I_{11} J_1 + r^I_{12} J_2 \tag{2.45}$$
$$X_2^I = r^I_{2q} J_q'^V + r^I_{21} J_1 + r^I_{22} J_2 \tag{2.46}$$

where the r's express the resistivities.

2.5.2 Diffusion films

For the liquid and vapor films in the system, the local entropy production can be written for $P = L, V$:

$$\sigma^P = J_q'^P X_q'^{P,loc} + J_1 X_1^{P,loc} + J_2 X_2^{P,loc} \tag{2.47}$$

A derivation of this expression is given in appendix A.1.2 where the following local driving forces are obtained:

$$X_q'^{P,loc} = \frac{d}{dx}\left(\frac{1}{T^P}\right) \tag{2.48}$$
$$X_1^{P,loc} = -\frac{1}{T^P}\frac{d\mu_{1,T}(T^P)}{dx} \tag{2.49}$$
$$X_2^{P,loc} = -\frac{1}{T^P}\frac{d\mu_{2,T}(T^P)}{dx} \tag{2.50}$$

The local driving forces can be written as:

$$X_q'^{P,loc} = r^P_{qq} J_q'^P + r^P_{q1} J_1 + r^P_{q2} J_2 \tag{2.51}$$
$$X_1^{P,loc} = r^P_{1q} J_q'^P + r^P_{11} J_1 + r^P_{12} J_2 \tag{2.52}$$
$$X_2^{P,loc} = r^P_{2q} J_q'^P + r^P_{21} J_1 + r^P_{22} J_2 \tag{2.53}$$

To find the total entropy production of the diffusion films, the integral over the film thickness is taken:

$$\frac{dS^{irr,P}}{dt} = \int_{\delta^P} \sigma^P dx = J_q'^P X_q'^P + J_1 X_1^P + J_2 X_2^P \tag{2.54}$$

where δ^P is the thickness of the diffusion film of phase P. We assume here that the value of the enthalpy of the mass streams does not vary due to temperature gradient over the diffusion film. We then have that the measurable heat flux is constant throughout the film.

By assuming constant local driving forces and resistivities, the total driving forces for the films can be written:

$$X_q'^P = \delta^P X_q'^{P,loc} = \bar{r}^P_{qq} J_q'^P + \bar{r}^P_{q1} J_1 + \bar{r}^P_{q2} J_2 \tag{2.55}$$
$$X_1^P = \delta^P X_1^{P,loc} = \bar{r}^P_{1q} J_q'^P + \bar{r}^P_{11} J_1 + \bar{r}^P_{12} J_2 \tag{2.56}$$
$$X_2^P = \delta^P X_2^{P,loc} = \bar{r}^P_{2q} J_q'^P + \bar{r}^P_{21} J_1 + \bar{r}^P_{22} J_2 \tag{2.57}$$

where $\bar{r}^P = \delta^P r^P$. Note that one common film is defined for all the transport processes in each phase. The thickness of this film vary with different operating conditions in the column.

2.5.3 Total system

The total entropy production of the system is the sum of the entropy production for each of the subsystems. Equation 2.39, 2.40 and 2.54 give:

$$\frac{dS^{irr}}{dt} = J_q'^V(X_q'^V + X_q'^I) + J_q'^L X_q^L + J_1(X_1^V + X_1^I + X_1^L) + J_2(X_2^V + X_2^I + X_2^L) \tag{2.58}$$

The measurable heat flux in the liquid, $J_q'^L$, can be eliminated using the energy balance for the interface:

$$J_q'^L = J_q'^V + J_1\Delta_{vap}H_1 + J_2\Delta_{vap}H_2 \tag{2.59}$$

This gives:

$$\begin{aligned}\frac{dS^{irr}}{dt} &= J_q'^V(X_q'^V + X_q'^I + X_q'^L) \\ &\quad + J_1(X_1^V + X_1^I + X_1^L + \Delta_{vap}H_1X_q'^L) \\ &\quad + J_2(X_2^V + X_2^I + X_2^L + \Delta_{vap}H_2X_q'^L) \\ &= J_q'^V X_q' + J_1X_1 + J_2X_2 \end{aligned} \tag{2.60}$$

Then we have that the driving forces for the whole system are:

$$X_q' = X_q'^V + X_q'^I + X_q'^L \tag{2.61}$$
$$X_1 = X_1^V + X_1^I + X_1^L + \Delta_{vap}H_1X_q'^L \tag{2.62}$$
$$X_2 = X_2^V + X_2^I + X_2^L + \Delta_{vap}H_2X_q'^L \tag{2.63}$$

The relationship between the fluxes and the overall forces can be written:

$$X_q' = r_{qq}J_q'^V + r_{q1}J_1 + r_{q2}J_2 \tag{2.64}$$
$$X_1 = r_{1q}J_q'^V + r_{11}J_1 + r_{12}J_2 \tag{2.65}$$
$$X_2 = r_{2q}J_q'^V + r_{21}J_1 + r_{22}J_2 \tag{2.66}$$

where the $\bar{r}$'s are overall coefficients for the entire system. By filling in the expressions for the forces in equation 2.61 - 2.63 and comparing with equation 2.64 - 2.66, the following expressions for the resistivities can be found, where the reciprocal relations are still fulfilled:

$$r_{qq} = \bar{r}_{qq}^V + r_{qq}^I + \bar{r}_{qq}^L \tag{2.67}$$
$$r_{q1} = \bar{r}_{1q} = \bar{r}_{q1}^V + r_{q1}^I + \bar{r}_{q1}^L + \bar{r}_{qq}^L\Delta_{vap}H_1 \tag{2.68}$$
$$r_{q2} = \bar{r}_{2q} = \bar{r}_{q2}^V + r_{q2}^I + \bar{r}_{q2}^L + \bar{r}_{qq}^L\Delta_{vap}H_2 \tag{2.69}$$
$$r_{11} = \bar{r}_{11}^V + r_{11}^I + \bar{r}_{11}^L + 2\Delta_{vap}H_1\bar{r}_{q1}^L + \Delta_{vap}H_1^2\bar{r}_{qq}^L \tag{2.70}$$
$$r_{22} = \bar{r}_{22}^V + r_{22}^I + \bar{r}_{22}^L + 2\Delta_{vap}H_2\bar{r}_{q2}^L + \Delta_{vap}H_2^2\bar{r}_{qq}^L \tag{2.71}$$
$$r_{12} = \bar{r}_{21} = \bar{r}_{12}^V + r_{12}^I + \bar{r}_{12}^L + \Delta_{vap}H_2\bar{r}_{q1}^L + \Delta_{vap}H_1\bar{r}_{q2}^L + \Delta_{vap}H_1\Delta_{vap}H_2\bar{r}_{qq}^L \tag{2.72}$$

In order to have expressions for the fluxes equation 2.64 - 2.66 can be rewritten:

$$\begin{bmatrix} J_q'^V \\ J_1 \\ J_2 \end{bmatrix} = \begin{bmatrix} r_{qq} & r_{q1} & r_{q2} \\ r_{1q} & r_{11} & r_{12} \\ r_{2q} & r_{21} & r_{22} \end{bmatrix}^{-1} \begin{bmatrix} X_q' \\ X_1 \\ X_2 \end{bmatrix} \tag{2.73}$$

2.5.4 Resistivities

The interface resistivities can be found from kinetic theory. In kinetic theory ideal gas is assumed, and the molecules are treated like hard spheres. For the interface it is also assumed a thickness of approximately one Knudsen layer, or one mean free path. The expressions for a binary mixture used by Kjelstrup and de Koeijer [11], corrected for misprints in Bedeaux et al [3], are:

$$\begin{aligned} r^I_{qq} &= \frac{\sqrt{\pi}}{4c^V R(T^V)^2 v_{mp}} \\ &\quad \times \left[1 + \frac{104}{25\pi}\left[\left(\frac{y^I_1\lambda^V_1}{\lambda^V}\right)^2\left(1 + \frac{c^V_2}{c^V_1}\sqrt[4]{\frac{M_1}{M_2}}\right) + \left(\frac{y^I_2\lambda^V_2}{\lambda^V}\right)^2\left(1 + \frac{c^V_1}{c^V_2}\sqrt[4]{\frac{M_2}{M_1}}\right)\right]\right] \quad (2.74) \\ r^I_{q1} &= r^I_{1q} = \frac{\sqrt{\pi}}{8c^V T^V v_{mp}}\left[1 + \frac{16y^I_1\lambda^V_1}{5\pi\lambda^V}\left(1 + \frac{c^V_2}{c^V_1}\sqrt[4]{\frac{M_1}{M_2}}\right)\right] \quad (2.75) \\ r^I_{q2} &= r^I_{2q} = \frac{\sqrt{\pi}}{8c^V T^V v_{mp}}\left[1 + \frac{16y^I_2\lambda^V_2}{5\pi\lambda^V}\left(1 + \frac{c^V_1}{c^V_2}\sqrt[4]{\frac{M_2}{M_1}}\right)\right] \quad (2.76) \\ r^I_{11} &= \frac{R\sqrt{\pi}}{16c^V v_{mp}} \times \left[1 + 32\left(\frac{1}{\sigma_1} + \frac{1}{\pi} - \frac{3}{4}\right)\left(1 + \frac{c^V_2}{c^V_1}\sqrt[4]{\frac{M_1}{M_2}}\right)\right] \quad (2.77) \\ r^I_{22} &= \frac{R\sqrt{\pi}}{16c^V v_{mp}} \times \left[1 + 32\left(\frac{1}{\sigma_2} + \frac{1}{\pi} - \frac{3}{4}\right)\left(1 + \frac{c^V_1}{c^V_2}\sqrt[4]{\frac{M_2}{M_1}}\right)\right] \quad (2.78) \\ r^I_{12} &= r^I_{21} = \frac{R\sqrt{\pi}}{16c^V v_{mp}} \quad (2.79) \end{aligned}$$

where λ is thermal conductivity, M is molar mass and σ_i is the condensation coefficient, meaning the fraction of component i that stays in the interface after collision. v_{mp} is the average of the most probable velocities of the components given by:

$$v_{mp} = \frac{1}{c^V}\left(c^V_1\sqrt{\frac{2RT^V}{M_1}} + c^V_2\sqrt{\frac{2RT^V}{M_2}}\right) \quad (2.80)$$

Resistivities for the diffusion films can be found from Maxwell-Stefan diffusivities, thermal conductivities and Soret coefficients. This is shown in appendix A.2. The derived relations are:

$$\begin{aligned} r^P_{qq} &= \frac{1}{\lambda^P(T^P)^2} \quad (2.81) \\ r^P_{1q} &= -z^P_2 r^P_{qq} s_T\left(\frac{\partial \ln\phi}{\partial \ln z^P_1} + 1\right)R(T^P)^2 \quad (2.82) \\ r^P_{2q} &= -\frac{z^P_1}{z^P_2} r^P_{1q} \quad (2.83) \\ r^P_{11} &= \frac{Rz^P_2}{z^P_1 c^P \bar{D}^P_{12}} + \frac{{r^P_{1q}}^2}{r^P_{qq}} \quad (2.84) \\ r^P_{12} &= -\frac{z^P_1}{z^P_2} r^P_{11} \quad (2.85) \\ r^P_{22} &= -\frac{z^P_1}{z^P_2} r^P_{12} \quad (2.86) \end{aligned}$$

where $P = Vb, Lb$.

2.5.5 Chemical potentials

The chemical potential of a liquid component i in equilibrium with an imaginary ideal vapor at the liquid interface temperature is:

$$\mu_i^L(T^{LI}) = \mu_i^{V,0}(T^{LI}) + RT^{LI} \ln \frac{p_i^*(T^{LI})x_i}{p_0} \tag{2.87}$$

where p_i^* is the vapor pressure of the liquid component i. The chemical potential of an ideal vapor at the liquid interface temperature is:

$$\mu_i^V(T^{LI}) = \mu_i^{V,0}(T^{LI}) + RT^{LI} \ln \frac{p_i}{p_0} \tag{2.88}$$

This gives that:

$$-\frac{\Delta_{VI,LI}\mu_i(T^{LI})}{T^{LI}} = R \ln \frac{p_i}{p_i^*(T^{LI})x_i^I} \tag{2.89}$$

and we have:

$$X_i^I = R \ln \frac{p_i}{p_i^*(T^{LI})x_i^I} \tag{2.90}$$

for $i = 1, 2$. Here, the gas is assumed to be ideal. For a non-ideal gas, the pressure must be replaced by fugacity. If we assume constant resistivities and driving forces for the diffusion films, we have the same way as above that:

$$X_i^V = -R \ln \left(\frac{y^I}{y^{Vb}} \right) \tag{2.91}$$

$$X_i^L = -R \ln \left(\frac{x^{Lb}}{x^I} \right) \tag{2.92}$$

2.6 Comparison between the integrated interface approach and Taylor and Krishna's approach

In their approach Taylor and Krishna assume equilibrium at the interface and no coupling between heat and mass transport. This is equivalent to setting all interface resistivities and all coupling coefficients between heat and mass transport in the integrated interface approach to zero.

2.6.1 Mass transport

In appendix A.3 it is shown that when the Soret effect is neglected in the integrated interface equations, the mass transport equations for two components within one phase can be rewritten on the same form as Taylor and Krishna's mass transport equations:

$$J_{1,am}^P = -c^P \bar{D}_{12}^P \Gamma^P \frac{\partial z_1}{\partial x} \tag{2.93}$$

$$J_1^P = J_{1,am}^P + z_1 J_t^P \tag{2.94}$$

By comparing these equations with equation 2.16 - 2.19, it is clear that the only remaining difference between the two approaches is the coefficients. The Maxwell-Stefan diffusivity divided by film thickness is replaced with $-k$ in Taylor and Krishna's approach. This is valid also for systems with more than two components.

The binary mass transfer coefficients used by Taylor and Krishna are functions of tray design as well as operating conditions. In ChemSep a set of different empirical models are used for the binary mass transfer coefficients, and the model chosen for each case depend on the tray conditions. More can be read about this in The ChemSep Book [12]. In "Multicomponent Mass Transfer" [17], Taylor and Krishna start with describing diffusion in general with the Maxwell-Stefan equations. For diffusion in distillation, however, they choose to use the binary pair mass transfer coefficients.

2.6.2 Heat transport

When the Dufour effect is neglected the integrated interface equation for the measurable heat flux is equal to Fourier's law:

$$J_q'^P = -\lambda^P \frac{\Delta T}{\Delta x} \tag{2.95}$$

where Δx is the length difference.

The corresponding equation from Taylor and Krishna's approach is the measurable heat flux part from equation 2.28 and 2.29:

$$J_q'^{P,TK} = h\Delta T \tag{2.96}$$

The equations have the same form, but the heat conductivity divided by the film thickness in the integrated interface equation is replaced by $-h$ in Taylor and Krishna's equation. Taylor and Krishna calculate the heat transfer coefficients from analogies between heat and mass transfer such as the Chilton-Colburn analogy or penetration models. More can be read about this in "Multicomponent Mass Transfer" [17]. They recommend to correct the estimated heat transfer coefficients for the effects of mass transfer by multiplying with a correction factor. So first they neglect the Dufour effect, but then they correct for the mass transport effects through this factor.

Chapter 3

Methodology

The integrated interface approach was tested on a de-ethanizer column. This column was first modelled using ChemSep. Then the fluxes and temperature and mole fraction profiles of this column were calculated using this approach. The impact of the choice of diffusion film thicknesses and Soret coefficients was examined. The importance of including heat and mass coupling and non-equilibrium over the interface was analyzed.

The de-ethanizer that was used as test-case was an ethane-propane column with 5 trays. The column pressure was 12 bar throughout the column. The feed was vapor at 280 K and 12 bar with 0.05 kmol/s ethane and 0.15 kmol/s propane. An overview of physical properties calculated by ChemSep for each tray, and of the properties of the phase bulks calculated by ChemSep is given in apendix B. In the ChemSep model, the heater and condenser, tray 1 and 5, were modelled as equilibrium trays, while tray 2 - 4 were modelled as non-equilibrium trays. Thus only trays 2 - 4 are used here. The mixtures were assumed ideal.

3.1 Solving the integrated interface transport equations

To find the fluxes over the interface, the temperature and composition profiles must be found to be able to find the right resistivities. The bulk temperatures and compositions are already set and used as boundary conditions for the system. We assume constant resistivities within each phase, and use the mean temperature and composition of the phase to approximate them. Temperatures and compositions are assumed to vary linearly through each phase. The overall driving forces for phase P can be written:

$$X_q'^P = \Delta_{A,B} \frac{1}{T} \tag{3.1}$$

$$X_1^P = -R \ln \left(\frac{z_1^B}{z_1^A} \right) \tag{3.2}$$

$$X_2^P = -R \ln \left(\frac{z_2^B}{z_2^A} \right) \tag{3.3}$$

where A and B are the diffusion film borders from left to right.

We then have the following 9 unknown variables: $J_q'^V$, J_1, J_2, T^{VI}, $y^I(1)$, $y^I(2)$, T^{LI}, $x^I(1)$ and $x^I(2)$. From section 2.5, we see that the variables are determined if the following equations are

fulfilled:

$$\begin{bmatrix} J_q'^V \\ J_1 \\ J_2 \end{bmatrix} = \begin{bmatrix} r_{qq} & r_{q1} & r_{q2} \\ r_{1q} & r_{11} & r_{12} \\ r_{2q} & r_{21} & r_{22} \end{bmatrix}^{-1} \begin{bmatrix} X_q' \\ X_1 \\ X_2 \end{bmatrix} \tag{2.73}$$

$$X_q'^P = \bar{r}_{qq}^P J_q'^P + \bar{r}_{q1}^P J_1 + \bar{r}_{q2}^P J_2 \tag{2.55}$$
$$X_1^P = \bar{r}_{1q}^P J_q'^P + \bar{r}_{11}^P J_1 + \bar{r}_{12}^P J_2 \tag{2.56}$$
$$X_2^P = \bar{r}_{2q}^P J_q'^P + \bar{r}_{21}^P J_1 + \bar{r}_{22}^P J_2 \tag{2.57}$$

where equation 2.55 - 2.57 must be fulfilled both for the vapor and liquid phase. Alternatively the equation set for one of the phases can be replaced with the corresponding equations for the interface, equation 2.44 - 2.46. The forces are functions of interface temperature and composition, see equation 3.1 - 3.3.

These equations were solved iteratively, with a procedure explained below using matlab. An overview of the procedure is given in figure 3.1. First initial guesses for the profiles were made. Here the interface temperature and mole fractions from ChemSep's solution of the system were used, both at the vapor and the liquid side of the interface. These values were used to calculate the resistivities, r, see equations in section 2.5.4. Then the total forces, X, were calculated using equation 2.61 - 2.63. Here, only T^{LI} is a variable, since most of the interface properties cancel out and the bulk properties are constant. Next step is to calculate the fluxes, using equation 2.73. Then the vapor phase and liquid phase forces were calculated using equation 2.55 - 2.57. New temperatures and mole fractions were found from these forces, using equation 3.1 - 3.3. This procedure was repeated until convergence was obtained. The value of $J_q'^L$ was then calculated using equation 2.59.

In the calculation the values for densities, molar weight for mixture and diffusivities were taken from the ChemSep model for the exact same tray. The heat conductivities were taken for the correct temperatures from the databank in ChemSep. Ideal mixtures were assumed, and the Antoine model for vapor pressure was used. When calculating the interface resistivities, the condensation coefficients are set to 0.8. If nothing else is specified are the diffusion film thicknesses used 600 μm and 35 μm for the vapor and liquid film respectively. The Soret coefficients are $-6.0 \cdot 10^{-4}$ for the liquid, and from 0.0234 $\cdot 10^{-4}$ - $0.3617 \cdot 10^{-4}$ for the vapor.

The answers were checked for consistency in several ways. The calculated mole fractions were checked whether they summed to 1. It was checked whether Gibbs-Duhem's equation was fulfilled within the vapor and liquid diffusion film, and if the coupling coefficients calculated lie within their boundary values, see equation 2.7. The temperature and $\mu_{T,i}/(T)$ profiles were plotted, and inspection of these plots was also used to evaluate the answers.

The matlab program used was written such that different resistances can easialy be enlargened or neglected. In this project different cases with such assumptions are used in the calculations. These cases are labelled and explained in table 3.1.

3.2 Sensitivity to diffusion film thicknesses

The sensitivity to the choice of diffusion film thicknesses was analysed. Also an evaluation on what thicknesses to use further was done.

In ChemSep empirical relations for distillation columns are used to find the mass transfer coefficients. Thus the widths of the diffusion layers are not used in ChemSep, as the resistances of these layers are taken into account through the mass transfer coefficients. In order to find a rough approximation for the thicknesses of the diffusion layers, Fick's law was used together with values for diffusion fluxes, concentrations, mole fractions and molar diffusivities calculated by ChemSep, see appendix C. Based on this a selection of thicknesses was tested for one of the distillation trays. To be able to compare with ChemSep, the resistances from the interface and the coupling coefficients between heat and mass were neglected. The results were inspected, both concerning the values of the fluxes and the temperature and composition profiles. Only the

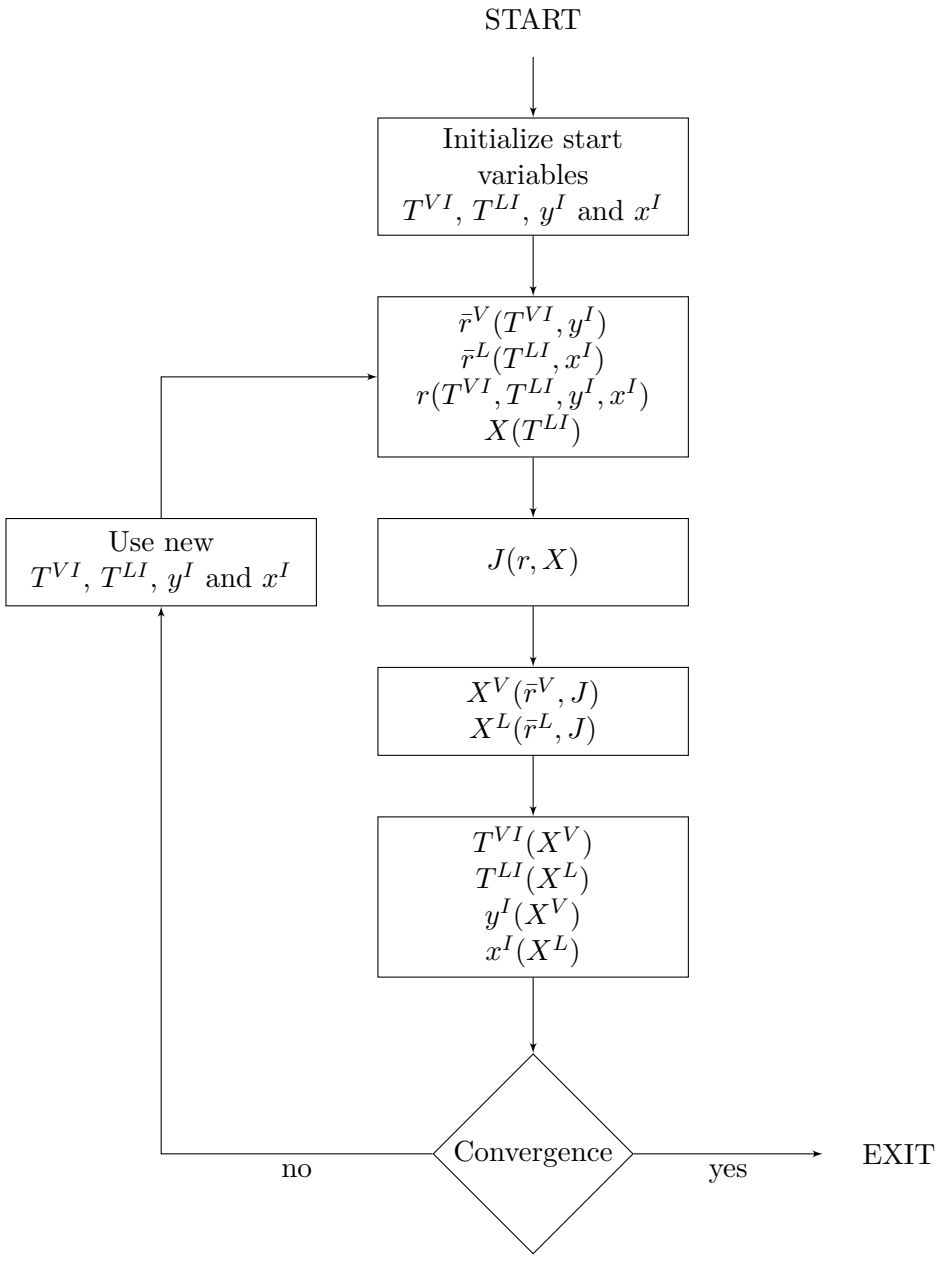

Figure 3.1: Flowchart over iteration method for finding fluxes and temperature and mole fraction profiles.

Table 3.1: Overview over cases with neglected or enlargened resistances used in this project.

Label	Explanation
Standard	No resistances are neglected or enlargened
$r_{ij}^I = 0$	The coupling between the two components in the interface is neglected
$r^I = 0$	All resistance in the interface is neglected
$r^I \cdot 10$	All resistance in the interface is multiplied with 10
$r_{qi}^P = 0$	The coupling between heat and mass in both diffusion layers is neglected

fluxes are of importance for importance for use in a distillation model, but the profiles provide information on whether the solution makes sense or not. Eventually one set of film thicknesses was chosen and tested for all the trays, both with the assumptions used above and with no assumptions, to see if it could be used for further calculations.

3.3 Sensitivity to Soret coefficient

The choice of Soret coefficients is based on data for similar mixtures to the ethane - propane mixture for the liquid coefficient, and on kinetic theory for the vapor coefficient, see appendix D. Higher and lower extreme values for the Soret coefficients were tested to see the influence from these values.

3.4 Assumptions on coupling and interface

The importance of including the coupling of heat and mass and the resistance of the interface was analyzed by neglecting these effects by setting the resistivities to zero and see if this changed the solution. First the coupling between the components in the interface was neglected. Then the entire interface was neglected. As this made almost no difference and the interface resistance used is for hard spherical molecules, also calculations with the interface resistance multiplied with 10 were done to check the influence of this. Eventually the coupling coefficients between heat and mass in the diffusion films were neglected, while the interface was included.

Chapter 4

Results and Discussion

4.1 Sensitivity to diffusion film thicknesses

The fluxes found for tray 2 with different film thicknesses and the same assumptions as ChemSep are listed in table 4.1 together with the fluxes calculated by ChemSep. The $(\mu_{T,i})/T$-, composition and temperature profiles are shown in figure 4.1 - 4.5. The profiles calculated for cases with the same film thickness ratios were identical, so only one figure is shown for each ratio. The $(\mu_{T,i})/T$ profiles vary so little that the variation is hard to see in the plots.

Table 4.1: Fluxes calculated with different film thicknesses and assuming no heat and mass coupling and no resistance in the interface for tray 2. The bottom line shows the fluxes calculated by ChemSep. The precision is reduced to two digits since this is enough to show the variation between the fluxes.

δ^V [μm]	δ^L [μm]	δ^L/δ^V	$J_q'^V$ [J/s]	$J_q'^L$ [J/s]	J_1 [mmol/s]	J_2 [mmol/s]
1200	700	0.58	$-4.8 \cdot 10^1$	$5.7 \cdot 10^2$	5.4	$4.0 \cdot 10^1$
1200	70	0.058	$1.4 \cdot 10^1$	$7.7 \cdot 10^2$	9.0	$4.7 \cdot 10^1$
1200	7	0.0058	$2.1 \cdot 10^1$	$2.1 \cdot 10^3$	$4.5 \cdot 10^1$	$1.2 \cdot 10^2$
120	700	5.8	$-3.2 \cdot 10^3$	$2.4 \cdot 10^3$	$6.0 \cdot 10^1$	$4.1 \cdot 10^2$
120	70	0.58	$-4.8 \cdot 10^2$	$5.7 \cdot 10^3$	$5.4 \cdot 10^1$	$4.0 \cdot 10^2$
120	7	0.058	$1.4 \cdot 10^2$	$7.7 \cdot 10^3$	$9.0 \cdot 10^1$	$4.7 \cdot 10^2$
12	700	58	$-5.0 \cdot 10^4$	$3.3 \cdot 10^3$	$6.7 \cdot 10^2$	$4.3 \cdot 10^3$
12	70	5.8	$-3.2 \cdot 10^4$	$2.4 \cdot 10^4$	$6.0 \cdot 10^2$	$4.1 \cdot 10^3$
12	7	0.58	$-4.8 \cdot 10^3$	$5.7 \cdot 10^4$	$5.4 \cdot 10^2$	$4.0 \cdot 10^3$
	ChemSep		$2.7 \cdot 10^2$	$6.7 \cdot 10^2$	$-5.5 \cdot 10^3$	$6.8 \cdot 10^3$

All the fluxes are inversely proportional to the film thicknesses as long as the ratios between the thicknesses are the same. This is in agreement with that a higher resistivity gives a lower flux. Since the local resistivities only are dependent on temperature and composition, and the

same ratios give the same profiles, the same local resistivities are obtained. As the resistance of the interface is neglected, we have that the total resistance is directly proportional to the film thicknesses.

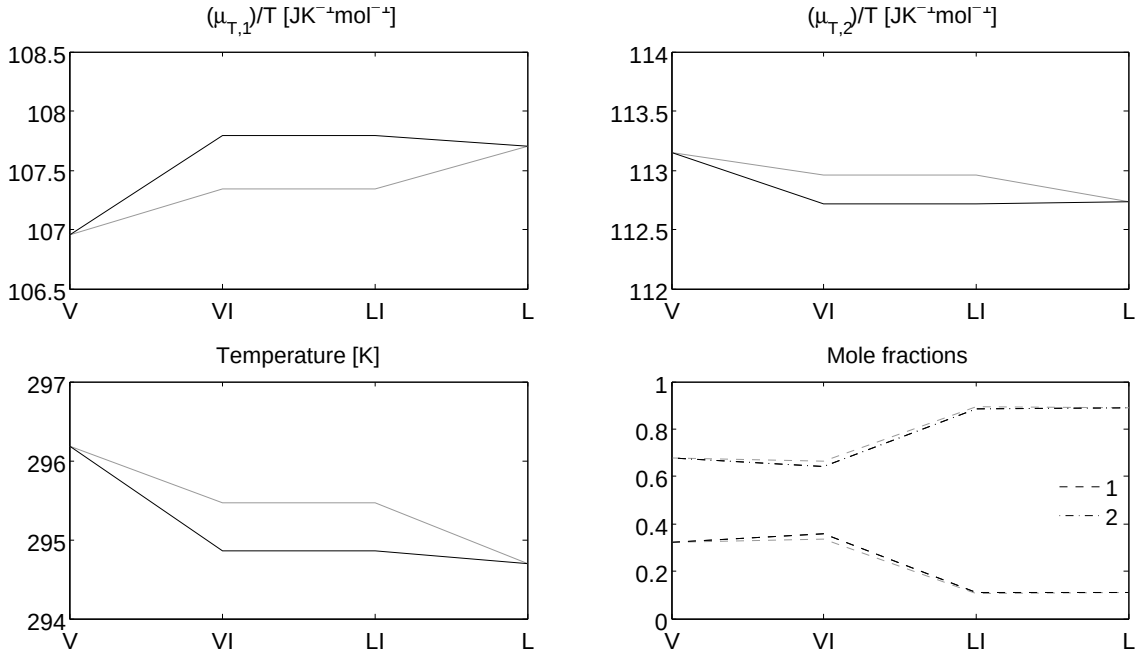

Figure 4.1: Profiles calculated for $\delta^L/\delta^V = 0.0058$ for tray 2. The calculated profiles are shown with black lines while the ChemSep profiles are grey. The mole fraction profile labelled 1 is for ethane while 2 is for propane.

The profiles are calculated from the values of X^V and X^L. As the interface resistivity is neglected, the overall resistivity matrix consists only of terms multiplied by δ^V and δ^L, see equation 2.67 - 2.72. The inverse of this 3×3 matrix has only terms multiplied with a factor consisting of two film thicknesses (δ^V or δ^L) divided by terms with tree such film thicknesses. This matrix is used to find the vector of fluxes, see equation 2.73. This means that the equations for the fluxes consist of only terms multiplied with two film thickness ratios divided by either δ^V or δ^L, thus the fluxes are dependent on the magnitude of the film thicknesses as commented above. When X^V and X^L are calculated from equation 2.55 - 2.57, all the terms will again be multiplied with δ^V or δ^L. This is why the profiles only are dependent on the film thickness ratio.

The interface temperatures lie between the vapor and liquid temperatures for ratio 0.0058 and 0.058, but it increases with increasing ratio, and at ratio 58 it is around 30 K higher than the vapor temperature.

For cases with high temperatures at the interface, the mole fractions at the liquid side of the interface do not sum to 1. This is a result of a vapor pressure model that performs badly at these temperatures. The Antoine vapor pressure model is used, and as the temperature rises it starts to predict vapor pressures for ethane that are too high. This gives mole fractions that are sometimes far too low at the liquid side of the interface, see equation 2.87. This again influences the liquid resistivities that are calculated, since they among other things are dependent on the mean mole fractions of the liquid phase. Through this, the bad performance of the vapor pressure model is responsible for some error in all the profiles and fluxes calculated for cases

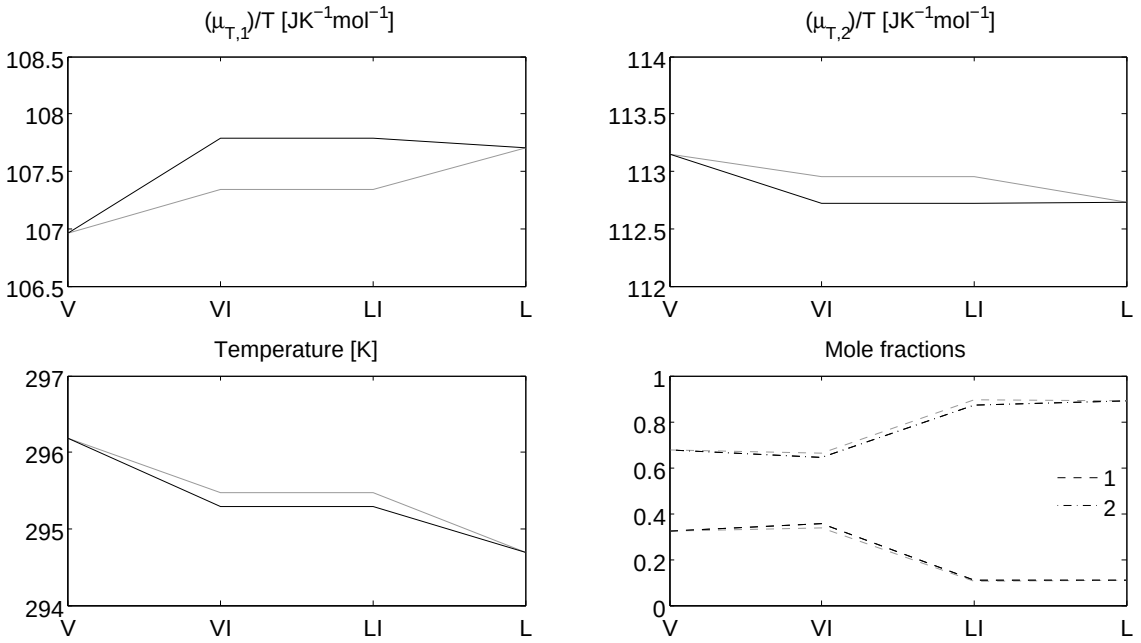

Figure 4.2: Profiles calculated for $\delta^L/\delta^V = 0.058$ for tray 2. The calculated profiles are shown with black lines while the ChemSep profiles are grey. The mole fraction profile labelled 1 is for ethane while 2 is for propane.

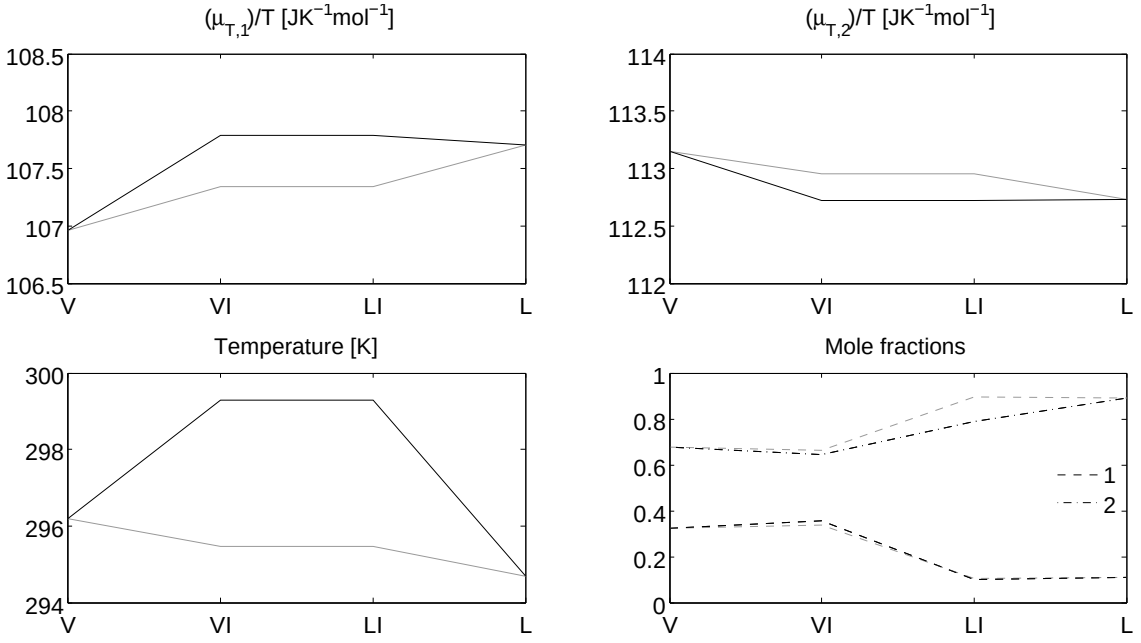

Figure 4.3: Profiles calculated for $\delta^L/\delta^V = 0.58$ for tray 2. The calculated profiles are shown with black lines while the ChemSep profiles are grey. The mole fraction profile labelled 1 is for ethane while 2 is for propane.

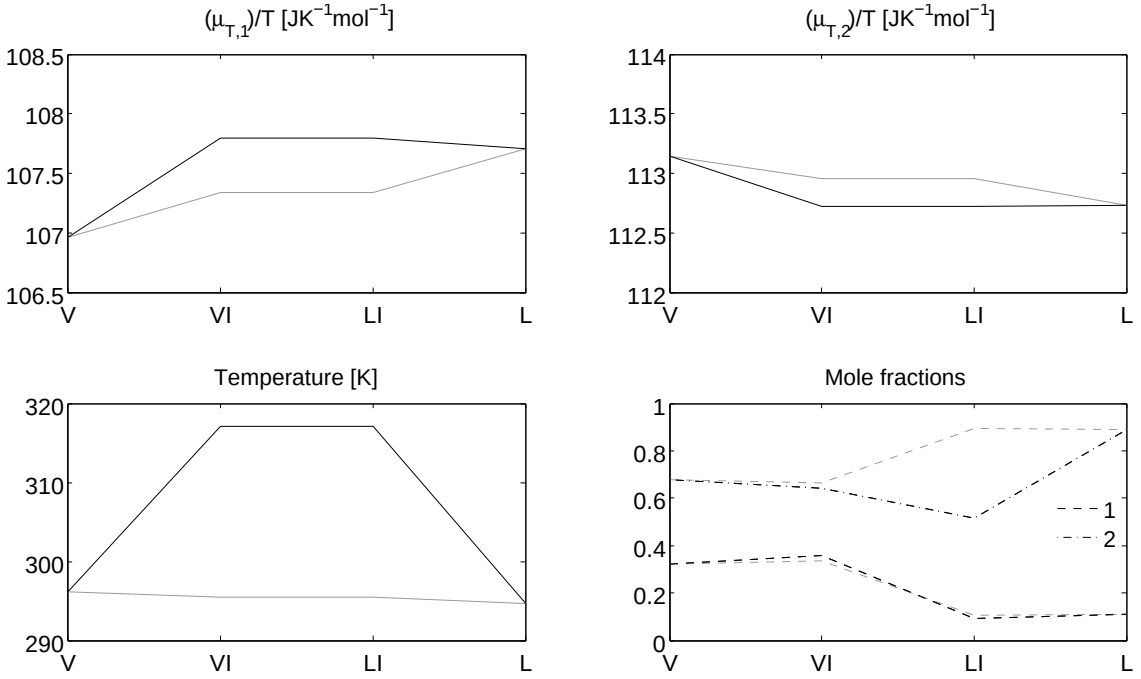

Figure 4.4: Profiles calculated for $\delta^L/\delta^V = 5.8$ for tray 2. The calculated profiles are shown with black lines while the ChemSep profiles are grey. The mole fraction profile labelled 1 is for ethane while 2 is for propane.

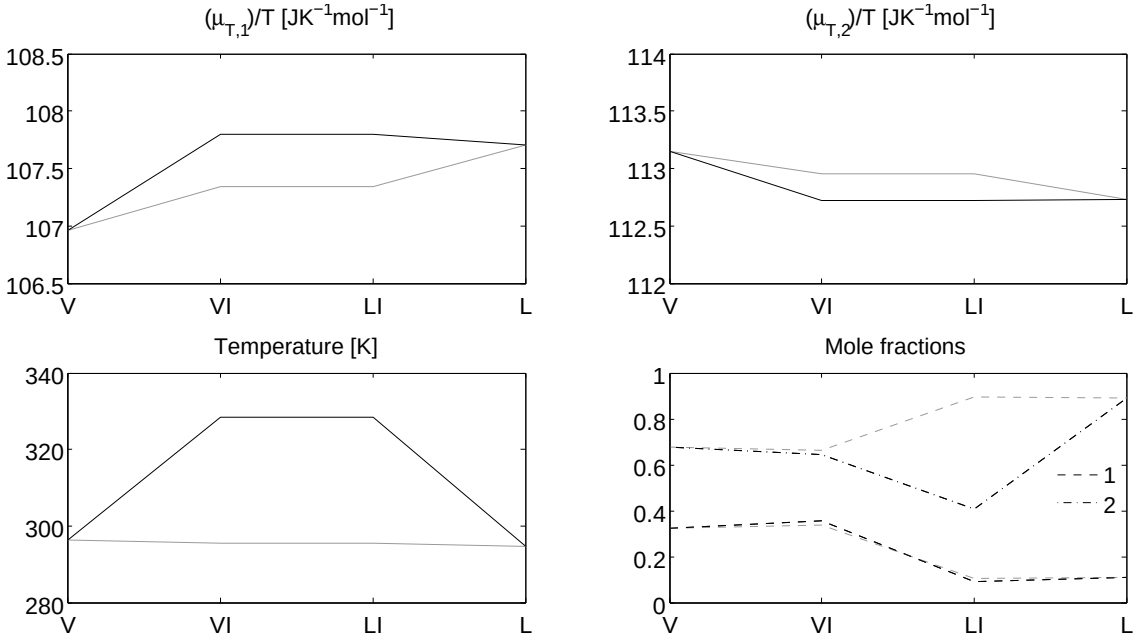

Figure 4.5: Profiles calculated for $\delta^L/\delta^V = 58$ for tray 2. The calculated profiles are shown with black lines while the ChemSep profiles are grey. The mole fraction profile labelled 1 is for ethane while 2 is for propane.

with this high temperatures. This error was first assumed to be small, so the equation was not replaced, but after checking this more thoroughly, it was shown to have a higher impact than first assumed, see appendix E.

4.1.1 Choosing film thicknesses for further calculations

The diffusion film thicknesses vary strongly with the geometry of the equipment and the hydraulics of the system. But as the choice of film thicknesses will imply a high level of uncertainty anyway, the thicknesses will be assumed to be constant throughout the column.

From the section above, we see that some film thickness ratios give very high temperature gradients through the systems. The most extreme case has a temperature rise on 30 K over 12 μm. Such temperature profiles can not appear in reality. The ratio $\delta^L/\delta^V = 0.058$ is the tested ratio that gives the profile closest to the profiles calculated by ChemSep. This ratio is chosen for further work. None of the cases tested in the previous section gave fluxes that all were close to the fluxes calculated by ChemSep. The case with 120 μm and 7 μm diffusion films give a heat flux at the vapor side that is in the same order of magnitude as the same flux calculated by ChemSep, while the case with 1200 μm and 70 μm give a heat flux at the liquid side that is not too far from the flux calculated by ChemSep. None of these have comparable mass fluxes, especially not for ethane. To be able to go on with the calculations, the thicknesses 600 and 35 μm is chosen for the vapor and the liquid film, respectively. This is a compromise between the two cases mentioned above, and it still has the thickness ratio 0.058. Both thicknesses are also within the intervals proposed by Bedeaux and Kjelstrup, see appendix C.

The chosen thicknesses are tested also for tray 3 and 4, both with the assumptions used by ChemSep and with all resistances included. This is to check that the thicknesses still can be used. The impact of the assumption and the still big difference from ChemSep's calculation is discussed later in this chapter. The fluxes of the tested thicknesses are listed in table 4.2. The profiles for tray 3 and 4 are shown in figure 4.6 - 4.7. The profiles for tray 2 are already shown in figure 4.3. Only the profiles for calculations with ChemSep assumptions are shown, because the differences between the profiles for this and for the calculation with all resistances included are minimal. Also for tray 3 and 4 the profiles look sensible, and they are quite close to the ChemSep profiles. The fluxes do not fit very well with the fluxes calculated by ChemSep, but compared to the other thicknesses tested for tray 2, they are ok. To be able to go on with the calculations, these film thicknesses are considered acceptable.

Table 4.2: Fluxes calculated for tray 2 - 4 with 600 and 35 μm for vapor and liquid film thicknesses, respectively. Calculations labelled "int int" are calculations done in this project with the integrated interface approach, while calculations labelled "ChemSep" are done by ChemSep. The numbers are given with three digits since this is the precision of the input numbers used in the integrated interface calculations.

Tray	Calculation	Assumptions	$J_q'^V$ [J/s]	$J_q'^L$ [J/s]	J_1 [mmol/s]	J_2 [mmol/s]
2	int int	Standard	$2.73 \cdot 10^1$	$1.54 \cdot 10^3$	$1.77 \cdot 10^1$	$9.35 \cdot 10^1$
	int int	$r^I = 0$, $r_{qi}^P = 0$	$2.78 \cdot 10^1$	$1.55 \cdot 10^3$	$1.79 \cdot 10^1$	$9.40 \cdot 10^1$
	ChemSep	$r^I = 0$, $r_{qi}^P = 0$	$2.75 \cdot 10^2$	$6.71 \cdot 10^2$	$-5.52 \cdot 10^3$	$6.79 \cdot 10^3$
3	int int	Standard	$7.16 \cdot 10^1$	$5.10 \cdot 10^3$	$6.87 \cdot 10^1$	$3.08 \cdot 10^2$
	int int	$r^I = 0$, $r_{qi}^P = 0$	$7.27 \cdot 10^1$	$5.14 \cdot 10^3$	$6.98 \cdot 10^1$	$3.09 \cdot 10^2$
	ChemSep	$r^I = 0$, $r_{qi}^P = 0$	$2.45 \cdot 10^2$	$6.71 \cdot 10^2$	$-2.31 \cdot 10^4$	$3.02 \cdot 10^4$
4	int int	Standard	$2.08 \cdot 10^1$	$5.82 \cdot 10^3$	$4.40 \cdot 10^1$	$3.85 \cdot 10^2$
	int int	$r^I = 0$, $r_{qi}^P = 0$	$2.05 \cdot 10^1$	$5.86 \cdot 10^3$	$4.46 \cdot 10^1$	$3.88 \cdot 10^2$
	ChemSep	$r^I = 0$, $r_{qi}^P = 0$	$2.35 \cdot 10^2$	$7.14 \cdot 10^2$	$-1.65 \cdot 10^4$	$2.29 \cdot 10^4$

4.2 Sensitivity to Soret coefficient

The choice of Soret coefficients is based only on data for a few similar mixtures for the liquid coefficient, and on kinetic theory for the vapor coefficient, see appendix D. To see how dependent the calculated fluxes are on these coefficients, calculations with values 10 times bigger than the values used are checked, and also calculations for this value with opposite sign. These values were compared with calculations with Soret coefficients equalling zero. The results are presented in table 4.3.

For variation of the vapor Soret coefficients, the measurable heat flux at the vapor side is 21 % higher for the high positive Soret coefficient than for zero Soret coefficient, and for the low negative value, the vapor measurable heat flux was 21 % lower than for zero Soret coefficient. The other fluxes changed only with less than 1 %. For variation of the liquid Soret coefficient, the vapor heat flux increased and decreased with around 3 % when using the extreme cases compared to coefficients equalling zero. The liquid heat flux increased and decreased with around 6 %. The ethane flux increased and decreased with around 15 %, while the propane flux increased and decreased with around 5 %. Equation 2.82 and 2.83 show how the heat and mass coupling parts of the equations are directly dependent on the Soret coefficients. The variations in the profiles caused by the different Soret coefficients are so small that they are not visible in the plots.

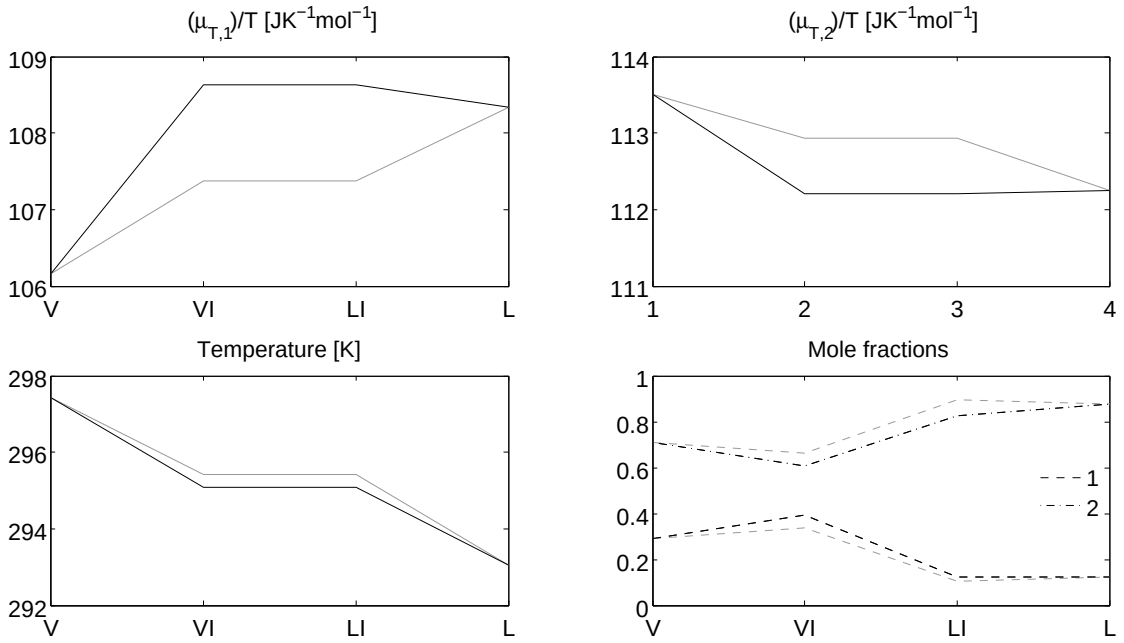

Figure 4.6: Profiles calculated for chosen film thicknesses with ChemSep assumptions for tray 3. The calculated profiles are shown with black lines while the ChemSep profiles are grey. The mole fraction profile labelled 1 is for ethane while 2 is for propane.

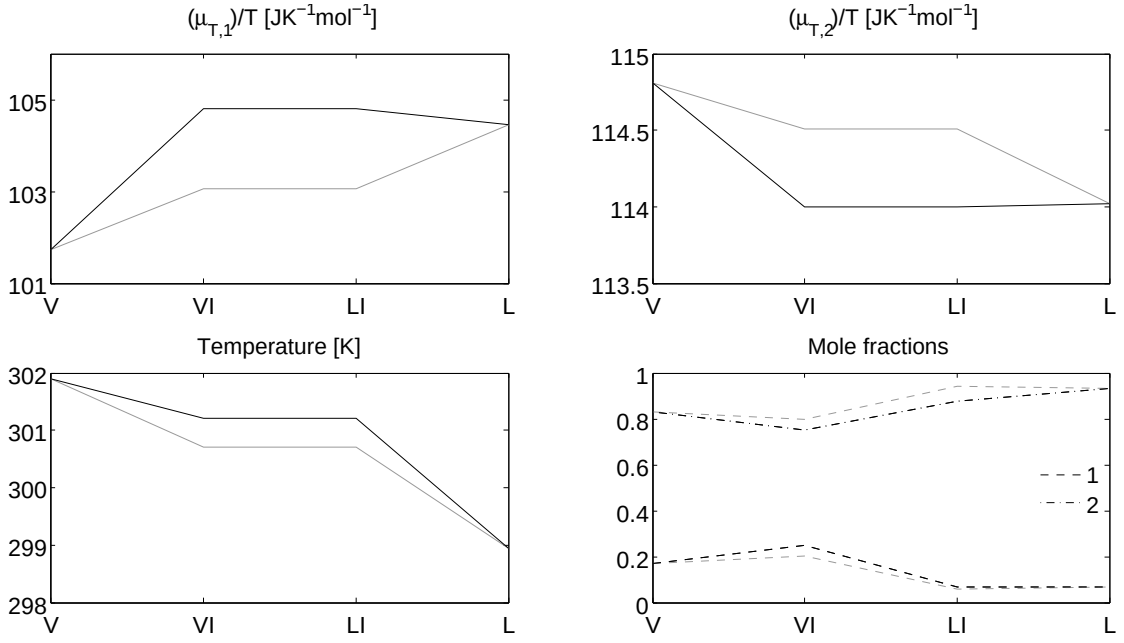

Figure 4.7: Profiles calculated for chosen film thicknesses with ChemSep assumtions for tray 4. The calculated profiles are shown with black lines while the ChemSep profiles are grey. The mole fraction profile labelled 1 is for ethane while 2 is for propane.

Table 4.3: Fluxes calculated for different Soret coefficients for tray 2. The numbers are given with three digits since this is the precision of the numbers used in the integrated interface calculations. s_T^V is the vapor Soret coefficient while s_T^L is the liquid Soret coefficient.

s_T^V	s_T^L	$J_q'^V$ [J/s]	$J_q'^L$ [J/s]	J_1 [mmol/s]	J_2 [mmol/s]
-4.00 $\cdot 10^{-4}$	- 6.00 $\cdot 10^{-4}$	33.6	$1.55 \cdot 10^3$	17.7	93.7
0	- 6.00 $\cdot 10^{-4}$	27.8	$1.54 \cdot 10^3$	17.7	93.5
4.00 $\cdot 10^{-4}$	- 6.00 $\cdot 10^{-4}$	22.1	$1.53 \cdot 10^3$	17.6	93.3
3.60 $\cdot 10^{-5}$	- 6.00 $\cdot 10^{-3}$	28.1	$1.46 \cdot 10^3$	15.5	89.2
3.60 $\cdot 10^{-5}$	0	27.3	$1.54 \cdot 10^3$	17.9	94.0
3.60 $\cdot 10^{-5}$	6.00 $\cdot 10^{-3}$	26.5	$1.64 \cdot 10^3$	20.6	99.2

4.3 Assumptions on coupling and interface

The fluxes calculated for tray 2 - 4 with different assumptions are listed in table 4.4. The differences between the results of each calculation and the same calculation with standard assumptions are also listed. When the coupling between the two components in the interface is neglected are the changes in the fluxes too small to be visible with tree digits accuracy. When all resistance in the interface is neglected, the calculated fluxes are changed with around 2 ‰ for the heat flux at the liquid side and for the ethane mass flux for tray 3. All the other fluxes had too small changes to be visible. When the interface resistances are multiplied with 10 are the fluxes changed with from -6.49 ‰ to 3.47 ‰. Neglecting all coupling between heat and mass in the two diffusion films changed the fluxes with -14.4 ‰ to 18.3 ‰.

The temperature, $(\mu_{T,i})/T$ and composition profiles calculated with the different assumptions gave so similar results that it is impossible to see the differences in the profile plots. The profiles for tray 2, 3 and 4 look all identical to the profiles in figure 4.2, 4.6 and 4.7. Figure 4.8 shows the temperature and $(\mu_{T,i})/T$ profiles for tray 2 when zoomed in dramatically so that only the interface area is shown and that it is possible to distinct the profiles from each other. All the profiles calculated for $r_{12}^I = 0$ and the profiles calculated with standard assumptions overlap even in this plot. The profile calculated with $r^I = 0$ is around 0.0001 K higher than the profile with standard assumptions in the temperature plot. In the $(\mu_{T,i})/T$ plots, the profiles lie around 50 μJK^{-1}mol^{-1} over and 30 μJK^{-1}mol^{-1} below the profile with standard assumptions. These profiles are all straight lines, as the assumption means that there must be equilibrium over the interface. The temperature and chemical potential have to be the same on each side. This implies that also the values for $(\mu_{T,i})/T$ must be the same on each side. The profiles for the calculations with the interface resisance multiplied with 10 have a higher slope than the others, since the higher resistance implies that the system is further away from equilibrium over the interface. For the temperature is the profile on the most 0.001 K lower than the profile with standard assumptions, and the $(\mu_{T,i})/T$ profiles are 0.0003 JK^{-1}mol^{-1} lower and around 0.0001 JK^{-1}mol^{-1} higher than the profile with standard assumptions. The profile calculated for $r_{qi}^P = 0$ lie around 0.004 K higher than the other profiles in the temperature plot. In the $(\mu_{T,i})/T$ plots, the profiles lie very close to the profiles for standard assumptions. Generally, the

Table 4.4: Fluxes calculated using different assumptions for tray 2 - 4. The columns labelled "Diff" give the difference of the foregoing flux from the same flux calculated without any assumptions. The values are given with three digits since this is the precision of the numbers used in the calculations.

Tray	Assumptions	$J_q'^V$ [J/s]	Diff [‰]	$J_q'^L$ [J/s]	Diff [‰]	J_1 [mmol/s]	Diff [‰]	J_2 [mmol/s]	Diff [‰]
2	Standard	27.3	-	$1.54 \cdot 10^3$	-	17.7	-	93.5	-
	$r_{12}^I = 0$	27.3	0.00	$1.54 \cdot 10^3$	0.00	17.7	0.00	93.5	0.00
	$r^I = 0$	27.3	0.00	$1.54 \cdot 10^3$	0.00	17.7	0.00	93.5	0.00
	$r^I \times 10$	27.3	0.00	$1.53 \cdot 10^3$	-6.49	17.6	-5.65	93.3	-2.14
	$r_{qi}^P = 0$	27.8	18.3	$1.55 \cdot 10^3$	6.49	17.9	11.3	94.0	5.35
3	Standard	71.6	-	$5.10 \cdot 10^3$	-	68.7	-	308	-
	$r_{12}^I = 0$	71.6	0.00	$5.10 \cdot 10^3$	0.00	68.7	0.00	308	0.00
	$r^I = 0$	71.6	0.00	$5.11 \cdot 10^3$	1.96	68.8	1.46	308	0.00
	$r^I \times 10$	71.6	0.00	$5.10 \cdot 10^3$	0.00	68.5	-2.91	307	-3.25
	$r_{qi}^P = 0$	72.7	15.4	$5.14 \cdot 10^3$	7.84	69.7	14.5	309	3.25
4	Standard	20.8	-	$5.82 \cdot 10^3$	-	44.0	-	385	-
	$r_{12}^I = 0$	20.8	0.00	$5.82 \cdot 10^3$	0.00	44.0	0.00	385	0.00
	$r^I = 0$	20.8	0.00	$5.82 \cdot 10^3$	0.00	44.0	0.00	385	0.00
	$r^I \times 10$	20.9	3.47	$5.80 \cdot 10^3$	-3.44	43.8	-4.54	384	-2.60
	$r_{qi}^P = 0$	20.5	-14.4	$5.85 \cdot 10^3$	5.15	44.6	13.6	388	7.79

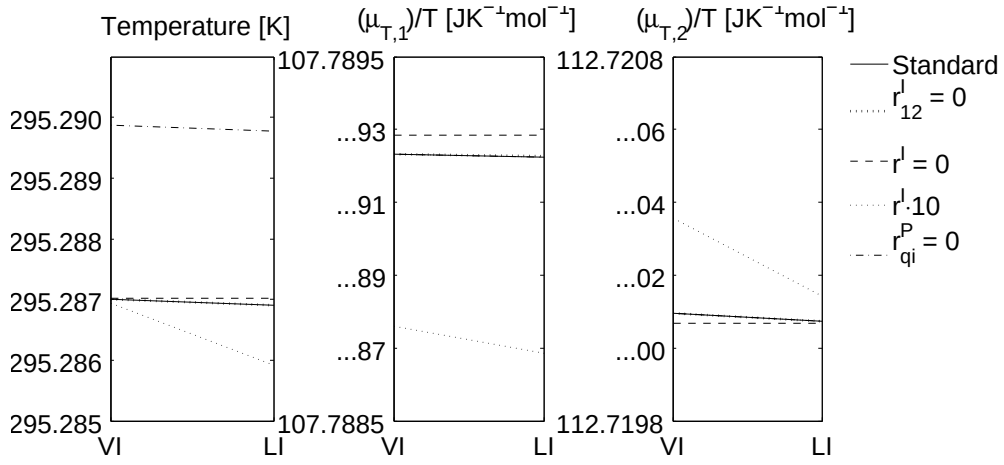

Figure 4.8: The interface profiles calculated with the different cases for tray 2. Mind that the ticks on the temperature and $(\mu_{T,i})/T$ axes change with very small steps.

differences caused by the assumptions taken here are minimal. For the fluxes, the assumption on neglecting the coupling between heat and mass has highest impact. The magnitude of this impact is dependent on the values of the Soret coefficients, which in this project have a high level of uncertainty. In the previous section we saw how the fluxes were much more influenced when higher values for the Soret coefficients were used.

The interface was expected to have a bigger impact on the calculations than what is seen here. To have a closer look on this, the contributions from the interface resistances to the overall resistances are calculated and plotted in table 4.5. It can be seen that for this system the interface contributions are all far less than 1 %. To multiply the interface resistances with 10 made more difference, but still not much.

Table 4.5: Interface contribution to overall resistance in tray 2. The values are given with three digits since this is the precision of the numbers used in the calculation.

Resistance	Overall	Interface	Interface contribution [%]
r_{qq}	$3.74 \cdot 10^{-7}$	$8.13 \cdot 10^{-12}$	$2.17 \cdot 10^{-3}$
r_{q1}	$2.08 \cdot 10^{-5}$	$8.89 \cdot 10^{-9}$	$4.28 \cdot 10^{-2}$
r_{q2}	$6.95 \cdot 10^{-5}$	$8.52 \cdot 10^{-9}$	$1.23 \cdot 10^{-2}$
r_{11}	$4.11 \cdot 10^{1}$	$3.70 \cdot 10^{-4}$	$9.01 \cdot 10^{-4}$
r_{22}	8.42	$2.27 \cdot 10^{-4}$	$2.70 \cdot 10^{-3}$
r_{12}	$-1.53 \cdot 10^{1}$	$5.27 \cdot 10^{-6}$	$-3.43 \cdot 10^{-5}$

For systems with other components, pressures and temperatures, can the influence of the interface to the overall resistance be higher. For instance are r^I_{q1} and r^I_{q2} inversely proportional to temperature, while $\bar{r}^P_{q1}$ and $\bar{r}^P_{q2}$ are temperature dependent only through the Soret coefficient and thermal conductivity. All the interface resistivities are dependent on pressure through the c^V-terms. They will all increase with decreasing pressure. $\bar{r}^P_{qq}$ is not dependent on pressure, and if the system is assumed ideal $\bar{r}^P_{1q}$ and $\bar{r}^P_{2q}$ are only pressure dependent through the Soret coefficient. In calculations done by Bock and van der Ham [4] for distillation of air, the heat fluxes became around twice and the mass fluxes half as big when neglecting the interface resistance compared to using standard assumptions. This is radically different from the results found here. The fluxes are calculated with a different approach, but the same assumptions can be checked. Air distillation operates with pressures just above 1 bar and temperatures around 85 K.

The relative influence from the resistivities in the diffusion films compared to the resistivities in the interface is also highly dependent on the chosen values of the film thicknesses. If lower film thicknesses are assumed, the resistances in the vapor and liquid films will be correspondingly lower. Thus the interface resistance will be responsible for more of the overall resistance.

4.4 Heat of transfer in interface

An interesting property of the interface is its high values for heats of transfer. If we write the general transport equations as fluxes, and rewrite to replace one of the component's mass force

in the heat flux equation with a mass flux, we have that:

$$J_q'^V = l_{qq}X_q + \frac{l_{q1}}{l_{11}}\left(J_1 - l_{1q}X_q - l_{12}X_2\right) + l_{q2}X_2 \tag{4.1}$$

The coefficient in front of the mass flux is the heat of transfer for this component. Kjelstrup and Bedeaux [10] have shown that for the interface is this coefficient related to the heat of evaporation, and therefore big. As we can see from the equation will the measurable heat flux then get a high contribution from the mass flux. The same is true also for the other component. This effect is especially important in the case of distillation, where it is a goal to achieve high mass fluxes across the interface. For the rest of the system is the heat of transfer not necessarily that big. In tray 2 in the distillation column considered here is the heat of transfer -1.11 $\cdot 10^3$ J/mol for component 1 in the interface, while it is -3.95 $\cdot 10^2$ J/mol for the overall system.

The three fluxes in the system can be looked upon as several fluxes in series. Since we have steady state, do the fluxes in the same series have the same magnitude, but each of them can have different contributions from other fluxes and forces. The fact that the properties of the transport through the interface is different than the transport through other phases do not influence the importance of including the interface resistance. This importance is only decided through the contribution of the interface resistances to the overall resistances.

4.5 Comparison with ChemSep

In table 4.2 we saw that the fluxes calculated by ChemSep deviate widely from the fluxes calculated here, even when the same assumptions are taken with respect to the interface and coupling between heat and mass. The differences within the solutions from the integrated interface approach caused by different assumptions are very small compared to the differences between the solutions of the two approaches. In section 2.6 we saw that with the same assumptions, the only differences between the two approaches are the coefficients used. Since we know that ChemSep has given good results compared to experiments, it is natural to assume that their coefficients give better results than the ones used in the integrated interface approach.

The ChemSep results give fluxes of the two components with different signs. The fluxes calculated here have the same sign, but the flux of ethane is smaller than the one for propane. The two different sets of fluxes predict very different separation properties of the column. The fluxes calculated by ChemSep give a better separation because in each tray, a net flux of ethane evaporate while propane condensate. The fluxes calculated here predict condensation of both ethane and propane. This will still give some separation, since taking the composition of the mixtures into account, more propane condensate than ethane.

The difference between the vapor and liquid measurable heat fluxes calculated is much higher than the difference between the same fluxes calculated by ChemSep. This is related to that ChemSep predicts just a small net condensation, while the calculations done here predict a high net condensation, see equation 2.59.

4.6 Error sources and uncertainity

In this project, some variables with a high level of uncertainity are used. The film thicknesses found as described above have a high level of uncertainity, and they have a high impact on

the system as seen in section 4.1. Using a 10 times higher or lower film thickness changed the order of magnitude or the sign of some of the fluxes, and the temperature and chemical potential profiles changed dramatically when different ratios between the thicknesses were used. Physical properties are taken from the ChemSep databank, and are related to a low level of uncertainity compared to this. The vapor pressure model was used outside its temperature limits, and is therefore the source of some error as discussed earlier in this chapter and in appendix E. It influenced the values of some of the resistivities and resistances. This however is of less importance than the uncertainity of the film thicknesses that have a direct impact on *all* the resistances, and have a higher level of uncertainity. The vapor pressure error was smaller in tray 2 than in tray 3 and 4. When assumptions are tested in section 4.3 the influence of the asumptions have around the same size for all trays, even though the error from the vapor pressure model is of diffent sizes. The choice of Soret coefficients is also related to a high level of uncertainity, but the highest and lowest Soret coefficients tested in section 4.2 only changed the fluxes within the same order of magnitude, and the changes in the temperatures and chemical potentials were not visible in the profile plots.

A general estimation of uncertainities in the calculated values is not done, since the film thicknesses seem to be of higher importance than anything else, and since it is hard to evaluate the uncertainity they contain.

4.7 Suggested directions for further work

Before further work with this project, all calculations should be done again with a better vapor pressure model, just to get rid of this error source. Then the approach should be tested on more systems, to get an overview on how big influence the interface and coupling between heat and mass have on different distillation systems. One start can be to look closer on air distillation, since Bock and van der Ham have found a high influence from the interface in this system. If the conclusion is that these things have an influence of importance, it is worth to work further with this.

Since the coefficients used by ChemSep are assumed to give better results for diffusion in distillation columns, a way to continue this work can be to use these coefficients in the integrated interface approach. If this is possible, we will have the advantage of the ChemSep coefficients that take the tray conditions and design into account, and that are shown to give good results, in addition to the advantage of including the effects of the interface and the coupling between heat and mass.

The ChemSep coefficients can be included in the integrated interface approach by deriving expressions for resistivities the same way as is done in appendix A.2, but by comparing with the transport equations used by ChemSep instead of Fourier's law and the Maxwell-Stefan equations. The expressions for these resistivities will contain the film thicknesses in the denominator. As the expressions later will be multiplied with the film thickness when the total resistances are found, the film thickness will cancel out. This means that the problem with finding good film thicknesses disappears. As an example the expression for r^P_{qq} found this way is shown below:

$$r^P_{qq}* = -\frac{1}{\delta^P h^P T^2} \tag{4.2}$$

where the * indicates that this is a resistivity found from Taylor and Krishna's equations.

The heat transfer coefficients used by ChemSep are corrected for the influence of the mass transfer with a correction factor. When used in the integrated interface approach, this factor must not be included, as the Dufour effect is taken into account through the coupling terms. Taylor and Krishna [17] write that such correction factors not are necessary to correct the mass transfer coefficients in distillation, so they have probably not used it on mass transport in ChemSep, but this has to be checked. It must also be checked whether effects from the interface somehow can be included in the coefficients, to make sure that this is not taken into account twice.

The long term goal with this project is to make a non-equilibrium model with the interface effects and coupling between heat and mass included. If the method proposed above gives good results, these transport equations can be included in Taylor and Krishna's non-equilibrium model instead of the equations they use.

Chapter 5

Conclusion

A method for calculating fluxes and temperature and chemical potential profiles over interfaces using non-equilibrium thermodynamics is established. Fluxes and profiles are calculated for a de-ethanizer column. It is found challenging to find reasonable values for film thicknesses and Soret coefficients. Both these values are shown to have a high impact on the solution, especially the film thicknesses. The fluxes calculated deviate widely from the same fluxes calculated by ChemSep. This deviation is concluded to come from different coefficients used in the transport equations. With the film thicknesses and Soret coefficients chosen, the coupling of heat and mass and the inclusion of resistance in the interface is shown to have only a small impact on the solution. Both neglecting the interface resistance and multiplying the interface resistance with 10 change the fluxes with less than 0.5 %. Neglecting the coupling of heat and mass transport changes the fluxes with less than 2 %. It is proposed to check this also for other distillation processes with other operating conditions, and a direction for further work is outlined.

Appendix A

Derivations

A.1 Entropy Production of Two-Component System

To be able to find equations for transport using non-equilibrium thermodynamics, the entropy production of the liquid diffusion layer, the interface and the vapor diffusion layer must be derived. The system has only transport of heat and mass, it is in a stationary state, and consists of c different components. Local equilibrium is assumed so the local thermodynamic state functions, expressed as densities, have the same values as they would have had in an equilibrium situation. The derivations below follows Kjelstrup and Bedeaux [10]. All fluxes are relative to the laboratory frame of reference.

A.1.1 Interface

A shematic overview of the interface with all fluxes entering and leaving is given in figure A.1.

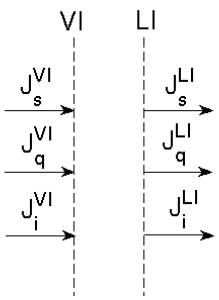

Figure A.1: Shematic overview over fluxes entering and leaving the interface.

The entropy balance for the interface can be written:

$$\frac{\partial s^I}{\partial t} = \frac{\partial S^{irr,I}}{\partial t} + J_s^{VI} - J_s^{LI} \tag{A.1}$$

where s is entropy density, J_s is entropy flux and $\frac{\partial S^{irr}}{\partial t}$ is the entropy production. Local equilibrium is assumed, thus the Gibbs equation must be valid, and for an interface element on

local form it is as follows:

$$du^I = T^I ds^I + \sum_{i=1}^{c} \mu_i^I d\Gamma_i \tag{A.2}$$

where u is internal energy density and Γ is the excess interface concentration. Rewriting and taking the time derivative of the entropy density gives:

$$\frac{\partial s^I}{\partial t} = \frac{1}{T^I}\frac{\partial u^I}{\partial t} - \frac{1}{T^I}\sum_{i=1}^{c} \mu_i^I \frac{\partial \Gamma_i}{\partial t} \tag{A.3}$$

The first law of thermodynamics gives for this system:

$$\frac{du^I}{dt} = J_q^{VI} - J_q^{LI} \tag{A.4}$$

where J_q is the total heat flux. The mass balance around the surface gives:

$$\frac{d\Gamma_i}{dt} = J_i^{VI} - J_i^{LI} \tag{A.5}$$

There are no chemical reactions in the system, only phase transformations. Mass enter and leave the surface as liquid at one side and as vapor at the other side. By inserting equation A.4 and A.5 in equation A.3, the following equation is obtained:

$$\frac{\partial s^I}{\partial t} = \frac{1}{T^I}(J_q^V - J_q^L) - \frac{1}{T^I}\sum_{i=1}^{c} \mu_i^I (J_i^V - J_i^L) \tag{A.6}$$

By rewriting the entropy balance, equation A.1, using that $J_s = \frac{1}{T}(J_q - \sum_{i=1}^{c} \mu_i J_i)$, and inserting equation A.6, we have that the entropy production is:

$$\frac{\partial S^{irr,I}}{\partial t} = J_q^L(\frac{1}{T^I} - \frac{1}{T^{LI}}) + J_q^V(\frac{1}{T^{VI}} - \frac{1}{T^I}) - \sum_{i=1}^{c} J_i^L(\frac{\mu_i^I}{T^I} - \frac{\mu_i^{LI}}{T^{LI}}) - \sum_{i=1}^{c} J_i^V(\frac{\mu_i^{VI}}{T^{VI}} - \frac{\mu_i^I}{T^I}) \tag{A.7}$$

The total heat fluxes consists of the measurable heats and the enthalpies of the mass fluxes:

$$J_q = J_q' + \sum_{i=1}^{c} H_i J_i \tag{A.8}$$

The term $\Delta_{LI,I}(\frac{\mu_i}{T})$ can be approximated using linearization the following way by using $-S_i = \left(\frac{\partial \mu_i}{\partial T}\right)_{p,n}$ and $\mu_i = H_i - TS_i$:

$$\begin{aligned}
\Delta_{LI,I}(\frac{\mu_i}{T}) &= \frac{\mu_i^I(T^I)}{T^I} - \frac{\mu_i^{LI}(T^{LI})}{T^{LI}} \\
&= \frac{\mu_i^I(T^I)}{T^I} - \frac{\mu_i^{LI}(T^I)}{T^I} + \frac{\mu_i^{LI}(T^I)}{T^I} - \frac{\mu_i^{LI}(T^{LI})}{T^{LI}} \\
&= \frac{1}{T^I}\Delta_{LI,I}\mu_{i,T}(T^I) + \left(\frac{\partial}{\partial T}\frac{\mu_i^{LI}}{T}\right)_{T=T^{LI}}(T^I - T^{LI}) \\
&= \frac{1}{T^I}\Delta_{LI,I}\mu_{i,T}(T^I) - \left(\frac{1}{T^{LI}}S_i^{LI} + \frac{\mu_i^{LI}}{(T^{LI})^2}\right)(T^I - T^{LI}) \\
&= \frac{1}{T^I}\Delta_{LI,I}\mu_{i,T}(T^I) + \left(S_i^{LI} + \frac{\mu_i^{LI}}{T^{LI}}\right)T^I\Delta_{LI,I}\left(\frac{1}{T}\right) \\
&= \frac{1}{T^I}\Delta_{LI,I}\mu_{i,T}(T^I) + H_i^{LI}\left(\frac{T^I}{T^{LI}}\right)\Delta_{LI,I}\left(\frac{1}{T}\right)
\end{aligned} \tag{A.9}$$

The ratio $\frac{T^I}{T^{LI}}$ can be approximated to 1, so that:

$$\Delta_{LI,I}(\frac{\mu_i}{T}) = \frac{1}{T^I}\Delta_{LI,I}\mu_{i,T}(T^I) + H_i^{LI}\Delta_{LI,I}\left(\frac{1}{T}\right) \tag{A.10}$$

By inserting equation A.8 and A.10 into equation A.7, the entropy production can be expressed the following way:

$$\frac{\partial S^{irr,I}}{\partial t} = J_q'^L\Delta_{LI,I}\frac{1}{T} + J_q'^V\Delta_{I,V}\frac{1}{T} + \sum_{i=1}^{c} J_i^L\left(-\frac{1}{T^I}\Delta_{LI,I}\mu_{i,T}(T^I)\right) + \sum_{i=1}^{c} J_i^V\left(-\frac{1}{T^I}\Delta_{I,VI}\mu_{i,T}(T^I)\right) \tag{A.11}$$

For a stationary state $J^L = J^V = J$. Then the above equation can be rewritten as:

$$\frac{\partial S^{irr,I}}{\partial t} = J_q'^L\Delta_{LI,I}\frac{1}{T} + J_q'^V\Delta_{I,VI}\frac{1}{T} + \sum_{i=1}^{c} J_i\left(-\frac{1}{T^I}\Delta_{LI,VI}\mu_{i,T}(T^I)\right) \tag{A.12}$$

Here the chemical potential differences are evaluated at the surface temperature. In a stationary state the total heat flux is constant throughout the system, giving the following relation:

$$J_q = J_q'^V + \sum_{i=1}^{c} H_i^V J_i = J_q'^L + \sum_{i=1}^{c} H_i^L J_i \tag{A.13}$$

By using this, the liquid heat flux in equation A.12 can be eliminated. Gibbs-Helmholtz' equation

$$\frac{\partial(\mu/T)}{\partial(1/T)} = H \tag{A.14}$$

can be used to rewrite the term expressing the force conjugate to the mass flux:

$$\begin{aligned}\frac{1}{T^I}\Delta_{LI,VI}\mu_{i,T}(T^I) &= \frac{1}{T^{LI}}\Delta_{LI,VI}\mu_{i,T}(T^{LI}) + \left(\frac{\partial}{\partial(1/T)}\left[\frac{\mu^{VI}(T) - \mu^{LI}(T)}{T}\right]\right)_{T=T^{LI}}\left(\frac{1}{T^I} - \frac{1}{T^{LI}}\right) \\ &= \frac{1}{T^{LI}}\Delta_{LI,VI}\mu_{i,T}(T^{LI}) + (H^{VI} - H^{LI})\left(\frac{1}{T^I} - \frac{1}{T^{LI}}\right)\end{aligned} \tag{A.15}$$

Now, the entropy production can be written:

$$\frac{\partial S^{irr,I}}{\partial t} = J_q'^V\Delta_{LI,VI}\left(\frac{1}{T}\right) + \sum_{i=1}^{c} J_i\left(-\frac{1}{T^{LI}}\Delta_{LI,VI}\mu_{i,T}(T^{LI})\right) \tag{A.16}$$

A.1.2 Diffusion Film

The derivation of the entropy production in the diffusion films follows the same procedure as the derivation for the interface. The entropy balance in a volume element in a homogeneous phase is given by:

$$\frac{\partial s^P}{\partial t} = \sigma^P - \frac{\partial}{\partial x}J_s^P \tag{A.17}$$

where σ is the local entropy production. Where $P = V, L$ and means that the variables belong to a volume element in the vapor or liquid diffusion films. Also here local equilibrium is assumed, and then we have Gibbs equation on local form for a volume element:

$$du^P = T^P ds^P + \sum_{i=1}^{c} \mu_i^P dc_i^P \tag{A.18}$$

Rewriting this and taking the time derivative of the entropy density gives:

$$\frac{\partial s^P}{\partial t} = \frac{1}{T^P}\frac{\partial u^P}{\partial t} - \frac{1}{T^P}\sum_{i=1}^{c}\mu_i^P\frac{\partial c_i^P}{\partial t} \tag{A.19}$$

From the first law of thermodynamics we have:

$$\frac{du^P}{dt} = -\frac{\partial}{\partial x}J_q^P \tag{A.20}$$

and a mass balance gives:

$$\frac{dc_i^P}{dt} = -\frac{\partial}{\partial x}J_i^P \tag{A.21}$$

By inserting equation A.20 and A.21 in equation A.19 we have:

$$\frac{\partial s^P}{\partial t} = -\frac{1}{T^P}\frac{\partial}{\partial x}J_q^P + \frac{1}{T^P}\sum_{i=1}^{c}\mu_i^P\frac{\partial}{\partial x}J_i^P \tag{A.22}$$

The entropy balance, equation A.17, can be rewritten using that $J_s = \frac{1}{T}(J_q - \sum_{i=1}^{c}\mu_i J_i)$ and inserting equation A.22. We then have that the entropy production is:

$$\sigma^P = J_q^P\frac{\partial}{\partial x}\frac{1}{T^P} + \sum_{i=1}^{c}J_i^P\left(-\frac{\partial}{\partial x}\frac{\mu_i^P}{T^P}\right) \tag{A.23}$$

We see from using the definition of derivation:

$$\frac{\partial}{\partial x}\frac{\mu_i^P}{T^P} = \lim_{\Delta x-->0}\frac{1}{\Delta x}\left(\frac{\mu_i^P\left(z_i(x+\Delta x), T(x+\Delta x)\right)}{T(x+\Delta x)} - \frac{\mu_i^P\left(z_i(x), T(x)\right)}{T(x)}\right) \tag{A.24}$$

where z_i is the mole fraction of component i of the phase in question, that the term can be approximated with linearization the same way as equation A.9. We then have that:

$$\frac{\partial}{\partial x}\frac{\mu_i^P}{T^P} = \frac{1}{T^P}\frac{\partial}{\partial x}\mu_{i,T}^P(T^P) + H_i^P\frac{\partial}{\partial x}\left(\frac{1}{T^P}\right) \tag{A.25}$$

where the subscript T indicates that the derivative of the term is taken with constant temperature. By using this and equation A.8 in equation A.23, the entropy production can be expressed as:

$$\sigma^P = J_q'^P\frac{\partial}{\partial x}\left(\frac{1}{T^P}\right) + \sum_{i=1}^{c}J_i^P\left(-\frac{\partial}{\partial x}\frac{\mu_{i,T}(T^P)}{T^P}\right) \tag{A.26}$$

A.2 Resistivities for Vapor and Liquid Phase

Values for the resistivities of the vapor and the liquid phase can be found from Maxwell-Stefan diffusion coefficients, thermal conductivity and Soret coefficients. Relations between the resistivities and these values are derived here, following Kjelstrup and Bedeaux [10].

From section 2.5.2 we have the following equations describing the fluxes and forces within a vapor or liquid layer:

$$\frac{d}{dx}\left(\frac{1}{T^P}\right) = r^P_{qq}J'^P_q + r^P_{q1}J_1 + r^P_{q2}J_2 \tag{A.27}$$

$$-\frac{1}{T^P}\frac{d\mu_{1,T}}{dx} = r^P_{1q}J'^P_q + r^P_{11}J_1 + r^P_{12}J_2 \tag{A.28}$$

$$-\frac{1}{T^P}\frac{d\mu_{2,T}}{dx} = r^P_{2q}J'^P_q + r^P_{21}J_1 + r^P_{22}J_2 \tag{A.29}$$

where superscript $P = V, L$ and indicates phase. These equations can be written in terms of velocities instead of component fluxes, where the velocity of component i is defined by $\mathrm{v}_i \equiv J_i/c_i$:

$$\frac{\partial}{\partial x}\frac{1}{T^P} = r'_{qq}J'^P_q + r'_{q1}\mathrm{v}_1 + r'_{q2}\mathrm{v}_2 \tag{A.30}$$

$$-\frac{c_1}{T^P}\frac{\partial\mu_{1,T}}{\partial x} = r'_{1q}J'^P_q + r'_{11}\mathrm{v}_1 + r'_{12}\mathrm{v}_2 \tag{A.31}$$

$$-\frac{c_2}{T^P}\frac{\partial\mu_{2,T}}{\partial x} = r'_{2q}J'^P_q + r'_{21}\mathrm{v}_1 + r'_{22}\mathrm{v}_2 \tag{A.32}$$

Written this way, the Onsager reciprocal relations hold also for the new resistivities. The relations between the new and old resistivities are:

$$\begin{aligned}
r'_{qq} &= r^P_{qq} & r'_{q1} &= r^P_{q1}c_1 & r'_{q2} &= r^P_{q2}c_2 \\
r'_{1q} &= r^P_{1q}c_1 & r'_{11} &= r^P_{11}c_1^2 & r'_{12} &= r^P_{12}c_1c_2 \\
r'_{2q} &= r^P_{21}c_2 & r'_{21} &= r^P_{21}c_1c_2 & r'_{22} &= r^P_{22}c_2^2
\end{aligned} \tag{A.33}$$

The sum of the left hand side of equation A.31 and A.32 is zero according to Gibbs-Duhem's equation. And as Onsager reciprocal relations apply, and equation A.30 - A.32 hold for any arbitrary measurable heat flux and component velocities, it follows that the resistivities in the matrix are dependent, and satisfy

$$\begin{aligned}
r'_{1q} + r'_{2q} &= 0 \\
r'_{11} + r'_{21} &= 0 \\
r'_{12} + r'_{22} &= 0
\end{aligned} \tag{A.34}$$

When the mass fluxes, or velocities, are zero, equation A.30 reduces to:

$$\frac{\partial}{\partial x}\frac{1}{T} = r'_{qq}J'^P_q \tag{A.35}$$

For simplicity the superscript indicating phase on temperature is suppressed. By comparing with Fourier's law,

$$J'^P_q = -\lambda^P\frac{\partial T}{\partial x} \tag{A.36}$$

where λ is the thermal conductivity of the mixture, and as equation A.30 is valid for all component velocities, the following relation is obtained:

$$r_{qq}^P = r'_{qq} = \frac{1}{\lambda^P T^2} \tag{A.37}$$

The Soret coefficient, s_T, which can be found from experiments, is the ratio between the thermal diffusion coefficient and the interdiffusion coefficient, and we have that:

$$s_{T1} = \frac{q_1^*}{c_1 T} \left(\frac{\partial \mu_{1,T}}{\partial c_1} \right)^{-1} \tag{A.38}$$

where q_i^* indicates measurable heat of transfer of component i and is given by:

$$q_j^* = -\frac{r_{qj}^P}{r_{qq}^P} \tag{A.39}$$

Rewritten, equation A.38 gives:

$$r_{1q} = -r_{qq} s_T c_1 T \frac{\partial \mu_{1,T}}{\partial c_1} \tag{A.40}$$

Differentiation of the chemical potential with respect to the concentration of component 1 gives:

$$\begin{aligned}
\frac{\partial \mu_{1,T}}{\partial c_1} &= \frac{\partial(\mu^0 + RT \ln(\phi x_1 p))}{\partial c_1} \\
&= RT \frac{\partial(\ln \phi + \ln x_1)}{\partial x_1} \frac{\partial(\frac{c_1}{c})}{\partial c_1} \\
&= RT \left(\frac{\partial \ln \phi}{\partial \ln x_1} \frac{\partial \ln x_1}{\partial x_1} + \frac{\partial \ln x_1}{\partial x_1} \right) \left(\frac{\frac{\partial c_1}{\partial c_1} c - \frac{\partial c}{\partial c_1} c_1}{c^2} \right) \\
&= RT \left(\frac{\partial \ln \phi}{\partial \ln x_1} \frac{1}{x_1} + \frac{1}{x_1} \right) \left(\frac{c - c_1}{c^2} \right) \\
&= \frac{RT}{x_1} \left(\frac{\partial \ln \phi}{\partial \ln x_1} + 1 \right) \frac{x_2}{c}
\end{aligned} \tag{A.41}$$

where p is the total pressure if the phase considered is vapor, and vapor pressure of component 1 if the phase is liquid. The vapor pressure is only dependent on temperature, and the total pressure is assumed constant. Using this in equation A.40 gives:

$$r_{1q}^P = -x_2 r_{qq}^P s_T \left(1 + \frac{\partial \ln \phi}{\partial \ln x_1} \right) RT^2 \tag{A.42}$$

From equations A.34 and A.33 we have that

$$r_{2q}^P = -\frac{x_1}{x_2} r_{1q}^P \tag{A.43}$$

For further analysis it is convenient to write equation A.30 - A.32 in the following form:

$$\frac{\partial T}{\partial x} = -\frac{1}{\lambda} \left(J'_q - c_1 q_1^* \mathrm{v}_1 - c_2 q_2^* \mathrm{v}_2 \right) \tag{A.44}$$

$$\frac{c_1}{T} \frac{\partial \mu_{1,T}}{\partial x} = -\frac{c_1 q_1^*}{T^2} \frac{\partial T}{\partial x} - R_{11} \mathrm{v}_1 - R_{12} \mathrm{v}_2 \tag{A.45}$$

$$\frac{c_2}{T} \frac{\partial \mu_{2,T}}{\partial x} = -\frac{c_2 q_2^*}{T^2} \frac{\partial T}{\partial x} - R_{21} \mathrm{v}_1 - R_{22} \mathrm{v}_2 \tag{A.46}$$

where

$$R_{jk} = r'_{jk} - \frac{r'_{jq} r'_{qk}}{r'_{qq}} \tag{A.47}$$

with $j, k = 1, 2$.

From equations A.34 and A.33 we have that:

$$\begin{aligned} c_1 q_1^* + c_2 q_2^* &= 0 \\ R_{11} + R_{12} &= 0 \\ R_{21} + R_{22} &= 0 \end{aligned} \tag{A.48}$$

The Maxwell-Stefan equations describe multi-component diffusion at constant temperature, and Krishna and Wesselingh [13] write them the following way for two components:

$$-\frac{\partial \mu_1}{\partial x} = \frac{RT}{\bar{D}_{12}} x_2 (\mathrm{v}_1 - \mathrm{v}_2) \tag{A.49}$$

$$-\frac{\partial \mu_2}{\partial x} = \frac{RT}{\bar{D}_{21}} x_1 (\mathrm{v}_2 - \mathrm{v}_1) \tag{A.50}$$

where $\bar{D}_{12}$ is the Maxwell-Stefan diffusivity for component 1 and 2. These coefficients can be used to describe multicomponent diffusion, but they are binary, and therefore easily available from experiments. They are symmetric, so $\bar{D}_{12} = \bar{D}_{21}$.

Equation A.45 and A.46 rewritten for constant temperature are:

$$-\frac{\partial \mu_{1,T}}{\partial x} = \frac{T}{c_1} R_{11} \mathrm{v}_1 + \frac{T}{c_1} R_{12} \mathrm{v}_2 \tag{A.51}$$

$$-\frac{\partial \mu_{2,T}}{\partial x} = \frac{T}{c_2} R_{21} \mathrm{v}_1 + \frac{T}{c_2} R_{22} \mathrm{v}_2 \tag{A.52}$$

Since equation A.45 and A.46 are fulfilled at any temperature gradient, we have from comparing equation A.49 - A.50 and A.51 - A.52 that:

$$\begin{aligned} R_{11} &= cR \frac{x_1 x_2}{\bar{D}_{12}} & R_{12} &= -cR \frac{x_1 x_2}{\bar{D}_{12}} \\ R_{21} &= -cR \frac{x_1 x_2}{\bar{D}_{12}} & R_{22} &= cR \frac{x_1 x_2}{\bar{D}_{12}} \end{aligned} \tag{A.53}$$

This is consistent with Onsager reciprocal relations and equations A.48. From these equations, equations A.33 and equation A.47 we have that:

$$r_{11}^P = \frac{R x_2}{x_1 c \bar{D}_{12}} + \frac{{r_{q1}^P}^2}{r_{qq}^P} \tag{A.54}$$

Equations A.33 and A.34 gives:

$$r_{12}^P = -\frac{x_1}{x_2} r_{11}^P \tag{A.55}$$

$$r_{22}^P = -\frac{x_1}{x_2} r_{12}^P \tag{A.56}$$

The expressions for the resistivities derived here are summarized in table A.1. The same expressions were derived by Kjelstrup and de Koeijer [11], following a somehow different track of derivation using the Maxwell-Stefan equations with temperature gradient.

Table A.1: Expressions for resistivities in the diffusion films

r^P_{qq}	$\frac{1}{\lambda^P T^2}$
r^P_{1q}	$-x_2 r^P_{qq} s_T \left(\frac{\partial \ln \phi}{\partial \ln x_1} + 1\right) RT^2$
r^P_{2q}	$-\frac{x_1}{x_2} r^P_{1q}$
r^P_{11}	$\frac{Rx_2}{x_1 c^P D^P_{12}} + \frac{{r^P_{1q}}^2}{r^P_{qq}}$
r^P_{12}	$-\frac{x_1}{x_2} r^P_{11}$
r^P_{22}	$-\frac{x_1}{x_2} r^P_{12}$

A.3 Rewriting the integrated interface mass transport equations

In order to describe mass transport within one phase, Taylor and Krishna find the diffusion relative to the average molar velocity, and from this the total mass transfer rate relative to a stationary interface:

$$J^{TK}_{1,am} = ck\Gamma\Delta z_i \tag{A.57}$$

$$J^{TK}_1 = J^{TK}_{1,am} + z_1 J_t \tag{A.58}$$

The Soret effect is neglected. k is a binary pair mass transfer coefficient. In this appendix is superscript indicating the phase suppressed for convenience.

The equations used by de Koeijer are given in a form directly relative to a stationary interface, see section 2.5. It is also possible to describe the same system with equations for the fluxes relative to the average molar velocity, and relate these fluxes to the stationary interface. These two equation sets are equivalent. The latter set is easier to compare with Taylor and Krishna's equations, and is therefore derived below.

This derivation is based on Kjelstrup and Bedeaux's discussion on how to use different frames of reference [10]. Here, a two-component system is considered, but the derivation can be extended to multicomponent systems.

When the average molar velocity is used as reference velocity, we have:

$$v_{ref} = v_{am} = z_1 v_1 + z_2 v_2 \tag{A.59}$$

Then we have the velocities of each component relative to the average molar frame of reference:

$$v_{1,am} = v_1 - v_{am} \tag{A.60}$$

$$v_{2,am} = v_2 - v_{am} \tag{A.61}$$

where v_1, v_2 and v_{am} are relative to the laboratory frame of reference. The corresponding fluxes are:

$$J_{1,am} = J_1 - c_1 v_{am} \tag{A.62}$$

$$J_{2,am} = J_2 - c_2 v_{am} \tag{A.63}$$

Using equation A.59, A.62 and A.63 we have:

$$J_{1,am} + J_{2,am} = 0 \tag{A.64}$$

The transport equation for component 1 can be written:

$$\frac{c_1}{T}\frac{\partial \mu_{1,T}}{\partial x} = -\frac{R_{11}}{c_1} J_{1,am} - \frac{R_{12}}{c_2} J_{2,am} \tag{A.65}$$

The equation for component 2 follows from Gibbs-Duhem equation. This equation is independent of frame of reference, since as we can see in appendix A.2:

$$R_{11} + R_{12} = 0 \tag{A.66}$$

Since the equation is independent of frame of reference, we can use the same relation between the Maxwell-Stefan diffusivities as used in appendix A.2:

$$R_{11} = cR\frac{x_1 x_2}{\bar{D}_{12}} \tag{A.67}$$

By using equation A.64, A.66, A.67 and rewriting we have that:

$$-\frac{1}{T}\frac{\partial \mu_{1,T}}{\partial x} = \frac{R}{c_1}\left(\frac{z_2}{\bar{D}_{12}} + \frac{z_1}{\bar{D}_{12}}\right) J_{1,am} \tag{A.68}$$

The chemical potential driving force can be rewritten to a mole fraction driving force:

$$\begin{aligned}
\frac{\partial \mu_{1,T}}{\partial x} &= \frac{\partial \mu_{1,T}}{\partial z_1}\frac{\partial z_1}{\partial x} \\
&= \frac{\partial}{\partial z_1}\left(\mu_i^0 + RT\ln(z_1\gamma_1 p)\right)\frac{\partial z_1}{\partial x} \\
&= RT\left(\frac{1}{z_1} + \frac{\partial \ln \gamma_1}{\partial z_1}\right)\frac{\partial z_1}{\partial x} \\
&= \frac{RT}{z_1}\left(1 + z_1\frac{\partial \ln \gamma_1}{\partial z_1}\right)\frac{\partial z_1}{\partial x} \\
&= \frac{RT}{z_1}\Gamma\frac{\partial z_1}{\partial x}
\end{aligned} \tag{A.69}$$

where p is the total pressure if this is the gas, and the vapor pressure of component 1 if this is the liquid. Γ is often called the thermodynamic factor, and for multicomponent systems it becomes a matrix with factors. When the system considered is ideal, the thermodynamic matrix is an identity matrix.

Using equation A.69 and rewriting equation A.68 we have that:

$$J_{1,am} = -c\bar{D}_{12}\Gamma\frac{\partial z_1}{\partial x} \tag{A.70}$$

Since $c_1 v_{am} = z_1 J_t$ where $J_t = J_1 + J_2$, we have from equation A.62 that:

$$J_1 = J_{1,am} + z_1 J_t \tag{A.71}$$

which can be used to find the fluxes relative to the stationary interface.

Appendix B

Properties provided by ChemSep

The properties of the phase bulks of each distillation tray used as boundary conditions for the calculated profiles are taken from the ChemSep model. These properties are listed in table B.1.

Table B.1: Properties of the phase bulks of each tray taken from the ChemSep model. Component 1 is ethane while component 2 is propane. The values are listed with the accuracy provided by ChemSep.

Property	Tray 2	Tray 3	Tray 4	Units
T^{Vb}	296.1878	297.4220	301.8949	K
T^{Lb}	294.6957	293.0536	298.9381	K
y_1^{Vb}	0.322084	0.292616	0.171869	-
x_2^{Vb}	0.677916	0.707384	0.828131	-
y_1^{Lb}	0.110894	0.123711	0.0689183	-
x_2^{Lb}	0.889106	0.876289	0.931082	-

Most of the physical properties used in the calculations are taken from the ChemSep model. The values of these properties are listed in table B.2.

Table B.2: Physical properties used in the calculations taken from ChemSep. The values are listed with the accuracy provided by ChemSep.

Property	Component	Tray 2	Tray 3	Tray 4	Units
Molar mass	ethane	$30.070 \cdot 10^{-3}$	$30.070 \cdot 10^{-3}$	$30.070 \cdot 10^{-3}$	kg/mol
	propane	$44.097 \cdot 10^{-3}$	$44.097 \cdot 10^{-3}$	$44.097 \cdot 10^{-3}$	kg/mol
Vapor thermal conductivity	ethane	$2.08 \cdot 10^{-2}$	$2.08 \cdot 10^{-2}$	$2.08 \cdot 10^{-2}$	J/(m^{2}s)
	propane	$1.74 \cdot 10^{-2}$	$1.74 \cdot 10^{-2}$	$1.74 \cdot 10^{-2}$	J/(m^{2}s)
Liquid thermal conductivity	ethane	$7.47 \cdot 10^{-2}$	$7.47 \cdot 10^{-2}$	$7.47 \cdot 10^{-2}$	J/(m^{2}s)
	propane	$9.39 \cdot 10^{-2}$	$9.39 \cdot 10^{-2}$	$9.39 \cdot 10^{-2}$	J/(m^{2}s)
Density vapor		19.3	19.4	19.9	kg/m^3
Density liquid		487	489	485	kg/m^3
Vapor mixture molar mass		$39.6 \cdot 10^{-3}$	$40.0 \cdot 10^{-3}$	$41.7 \cdot 10^{-3}$	kg/mol
Liquid mixture molar mass		$42.5 \cdot 10^{-3}$	$42.4 \cdot 10^{-3}$	$43.1 \cdot 10^{-3}$	kg/mol
Diffusivity vapor		$7.28 \cdot 10^{-7}$	$7.33 \cdot 10^{-7}$	$7.52 \cdot 10^{-7}$	m^2/s
Diffusivity liquid		$1.50 \cdot 10^{-8}$	$1.48 \cdot 10^{-8}$	$1.53 \cdot 10^{-8}$	m^2/s

Appendix C

Diffusion film

The thicknesses of the diffusion films in chemical processes are strongly related to chemical species, geometry of equipment and the hydraulics of the system. Thus, they vary with tray design and operating conditions. For distillation trays, the geometry is made such that as much contact between vapor and liquid as possible is obtained. This results in a complex mixture between vapor and liquid. Vapor enters the tray from below, first forming vapor jets or bubbles, froth and foam when the vapor is mixed with the liquid. Froth also enters from the tray above, and mixes with the rest. Figure C.1 gives a small impression on the complexity of the interfaces in the trays. It shows idealized views of distillation trays dominated by two different bubbling regimes.

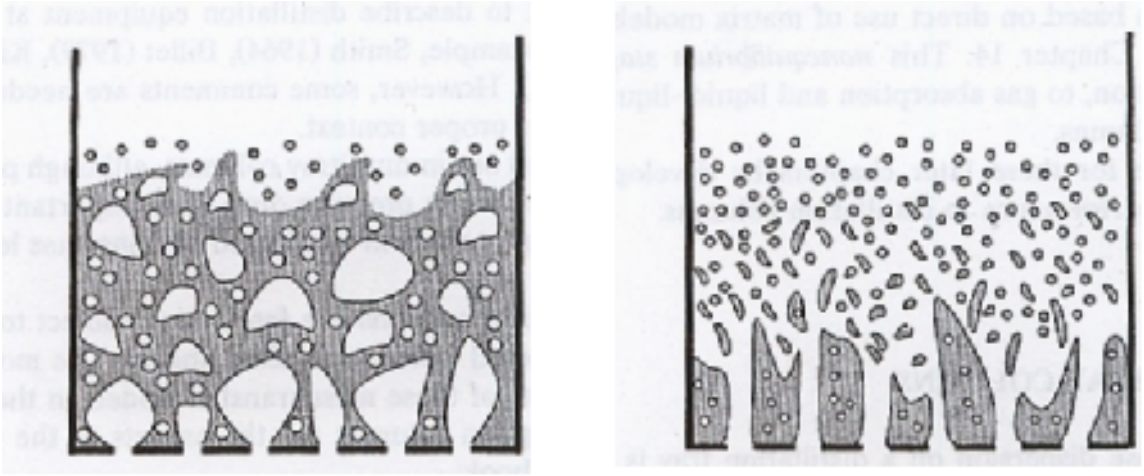

Figure C.1: Idealized views of the free bubbling regime and the spray regime on a distillation tray respectively. Taylor and Krishna, 1993 [17].

Often for such complex systems empirical relations for heat and mass transfer coefficients are used rather than diffusivities, heat conductivities and diffusion film thicknesses. In addition, heat and mass transport are usually considered separately, such that the diffusion films of the two types of transport not necessarily have the same thicknesses. This project considers coupling of processes, and thus *one* film thickness must be found for each phase.

De Koeijer [11] determined resistivities for distillation of water and ethanol. In lack of precise knowledge about the diffusion films, he used two different ratios between the liquid and vapor

film thicknesses. Then he found the liquid film thicknesses by fitting the entropy production of the system calculated from non-equilibrium transport equations to the entropy production from experimental data, where this value was the only adjustable variable in the fit. The first ratio was taken from the literature, Taylor and Krishna [17], where vapor controlled mass transfer is claimed to have a ratio between liquid and vapor film thickness around 0.001. The second ratio he found from using the thermal conductivity and Fick's diffusion coefficient, and this gave a ratio of 10. For more details about this, see the article cited above.

Bedeaux and Kjelstrup [2] write that the film thicknesses vary from 10^{-4} to 10^{-3} m for the vapor film and 10^{-5} to 10^{-4} m for the liquid film, refering to Taylor and Krishna [17].

To find approximate film thicknesses for this project, the column in question was modelled with ChemSep. In ChemSep empirical relations for distillation columns are used to find the heat and mass transfer coefficients, which corresponds to the thermal conductivities and diffusivities divided by the film thicknesses. Thus the width of the diffusion layers are not used explicitely in ChemSep, as they are taken into account through the heat and mass transfer coefficients. To find from this approximate film thicknesses, Fourier's and Fick's law were used. These equations are the most banal models for heat and mass transport, and no cross-effects are taken into account.

Fourier's law is given by:

$$J_q'^P = -\lambda^P \frac{\Delta T}{\delta_q^P} \tag{C.1}$$

where $J_q'^P$ is the measurable heat flux in phase P, λ^P is the thermal conductivity of phase P, ΔT is the temperature difference and δ_q is the thickness of the thermal diffusion film.

Fick's law is given by:

$$J_i^P = \frac{-cD_{ij}^P \Delta z_i}{\delta_\mu^P} \tag{C.2}$$

where J_i^P is the diffusion flux of component i in phase P, c is the total concentration, δ_μ^P is the mass diffusion film thickness, D_{ij}^P is the molar Fick's diffusivity of component i in component j in phase P and Δz_i is the mole fraction difference of component i.

Fick's law rewritten to find the mass diffusion film thicknesses given by:

$$\delta_\mu^P = \frac{-cD_{ij}\Delta x_i}{J_i} \tag{C.3}$$

All values on the right hand side can be found from the ChemSep model. ChemSep calculate D_{ij} because it is used in the empirical mass transfer coefficient model. The mass flux equations are based on the Maxwell-Stefan equations.

In ChemSep the heat flux was found with the following equation:

$$J_q'^P = -h^P \Delta T \tag{C.4}$$

where h^P is the heat transfer coefficient, which is found from analogies between heat and mass transport. By comparing equation C.4 with equation C.1 we see that the heat diffusion film thickness can be approximated with the following equation:

$$\delta_q^P = \frac{\lambda^P}{h^P} \tag{C.5}$$

Both λ^P and h^P are calculated by ChemSep, although only h^P is used directly in the heat transport equations.

The film thicknesses obtained this way are very approximate as they are found from Fick's and Fourier's equations, which are very simple models, using ChemSep, which again is another model. The film thicknesses will vary strongly within each distillation tray, and it can be seen in the sections below how they vary from tray to tray. But as the values found here are already not precise, the thicknesses will be treated as constant within each system modelled.

Film thicknesses approximated for the ethane-propane column, assuming ideal mixture, are given in table C.1. Based on these numbers, 120 μm and 70 μm are chosen as sensible values for the vapor and liquid film thickness, respectively. These thicknesses lay within the values given by Bedeaux and Kjelstrup, and the ratio between liquid and vapor film thickness is 1.7 which is close to de Koijer's second ratio. These values are used as basis for a number of values that are tested and compared, see section 4.1.

Table C.1: Diffusion film thicknesses

Colum stage	δ_μ^V μm	δ_q^V μm	δ_μ^L μm	δ_q^L μm
2	104	98.8	22.4	93.6
3	155	146	50.7	133
4	156	145	33.1	135

Appendix D

Soret Coefficient

D.1 Ethane-propane

Soret coefficients for ethane-propane mixtures at 12 bar and around 300 K are needed. An approximate value for the Soret coefficient of the liquid mixture is found from the measured thermal diffusion factors of two similar mixtures, see table D.1. The relation between the thermal diffusion factor and the Soret coefficient is:

$$\alpha_T = T s_T \tag{D.1}$$

Table D.1: Thermal diffusion factors and Soret coefficients for component 2 in two hydrocarbon mixtures

Component 1	Component 2	x_1	x_2	T [K]	p [bar]	α_{T2}	s_{T2}
Methane	Propane	0.34	0.66	346	40.5	0.79	$2.3 \cdot 10^{-3}$
n-hexane	*n*-octane	0.55	0.45	320	1	0.161	$5.03 \cdot 10^{-4}$

According to Kjelstrup and Bedeaux [10], the Soret effect is larger in liquids than in gases, and the magnitude increases the closer one comes to the critical point. The coefficient is smaller for mixtures with more similar molar weights and volumes. Also, the Soret coefficient is often positive for the lighter component and negative for the heavier. This does not apply to the mixtures in the table, and is therefore assumed to also not apply to the ethane-propane mixture.

To find an approximate Soret coefficient for the mixtures at 12 bar, an interpolation between the two coefficients as a function of pressure is done. Then, the value is 0.001. Since the value needed is for a mixture with a lower temperature, the coefficient should be a bit lower. Also the components are more similar in the ethane-propane mixture, than the mixtures in the table, so the Soret effect should be smaller. Thus eventually the Soret coefficient for propane in the ethane-propane mixture at 12 bar and around 300 K is assumed to be 0.0006, giving the value -0.0006 for ethane. The coefficient is also dependent on composition. For a methane-propane mixture the thermal diffusion factor varies between 0.65 and 12.51 due to this, see Kempers [8]. This is not taken into account for the value found here.

For the vapor mixture, the Soret coefficients were found using kinetic theory. The method used is described by Hirschfelder et. al. [6]. This gave the values in table D.2 for the ethane-propane column. These values show that the Soret coefficient vary a lot with the conditions on each tray. This indicates that the Soret coefficients found here, both for vapor and for liquid, only are rough estimates.

Table D.2: Vapor Soret coefficients for ethane calculated from kinetic theory

Column stage	s_T
2	$0.3617 \cdot 10^{-4}$
3	$0.3266 \cdot 10^{-4}$
4	$0.0235 \cdot 10^{-4}$

Appendix E

Discussion on error from vapor pressure model

The vapor pressure model used is the Antoine equation. For this model is the applicable temperature range not large, and it should never be used outside the stated temperature limits [16]. The upper temperature limit for ethane is 273.32 K. The temperatures used here are all higher than this. This has resulted in that the vapor pressure model predicts ethane vapor pressures that are too high, giving ethane mole fractions that are too low. Thus the mole fractions do not sum to unity. This can be seen in figure 4.3 - 4.5. The calculated mole fractions are used to find values for the resistivities. First the impact on these values were assumed to be small, so the model was not replaced. The temperatures used here are slighly higher than the critical temperature of ethane, so to find another way to estimate the mole fractions can be challenging. Later the impact of the mole fractions was checked more thoroughly, and shown to be higher than first assumed.

The influence on the whole system is hard to calculate, since the equations were solved iteratively. To get an impression of the influence, Gauss' law of error propagation was used to see how the error in the ethane mole fractions propagate to the resistivities and resistances.

The mole fractions used to find the resistivities, x^L, are the mean of the liquid interface and the liquid bulk mole fractions, x^{LI} and x^{Lb}. The error propagation in this can be written:

$$\sigma^2_{x_1^L} = \left(\frac{\partial x_1^L}{\partial x_1^{LI}}\right)^2 \sigma^2_{x_1^{LI}} = \left(\frac{1}{2}\right)^2 \sigma^2_{x_1^{LI}} \tag{E.1}$$

The error propagation in the liquid resistivities that depend on the liquid mole fraction is described with:

$$\sigma^2_{r^L_{2q}} = \left(\frac{\partial r^L_{2q}}{\partial x_1^L}\right)^2 \sigma^2_{x_1^L} = \left(r^L_{qq} s_T \left(\frac{\partial \ln \phi}{\partial \ln x_2} + 1\right) RT^2\right)^2 \sigma^2_{x_1^L} \tag{E.2}$$

$$\sigma^2_{r^L_{11}} = \left(\frac{\partial r^L_{11}}{\partial x_1^L}\right)^2 \sigma^2_{x_1^L} = \left(\frac{Rx_2}{2x_1^2 c^L \bar{D}^L_{12}}\right)^2 \sigma^2_{x_1^L} \tag{E.3}$$

$$\sigma^2_{r^L_{12}} = \left(\frac{\partial r^L_{12}}{\partial x_1^L}\right)^2 \sigma^2_{x_1^L} + \left(\frac{\partial r^L_{12}}{\partial r^L_{11}}\right)^2 \sigma^2_{r^L_{11}} = \left(-\frac{r^L_{11}}{x_2}\right)^2 \sigma^2_{x_1^L} + \left(-\frac{x_1}{x_2}\right)^2 \sigma^2_{r^L_{11}} \tag{E.4}$$

$$\sigma^2_{r^L_{22}} = \left(\frac{\partial r^L_{22}}{\partial x_1^L}\right)^2 \sigma^2_{x_1^L} + \left(\frac{\partial r^L_{22}}{\partial r^L_{12}}\right)^2 \sigma^2_{r^L_{12}} = \left(-\frac{r^L_{12}}{x_2}\right)^2 \sigma^2_{x_1^L} + \left(-\frac{x_1}{x_2}\right)^2 \sigma^2_{r^L_{12}} \tag{E.5}$$

This again propagates to the overall resistivities:

$$\sigma_{r_{q2}}^2 = \left(\frac{\partial r_{q2}}{\partial r_{q2}^L}\right)^2 \sigma_{r_{q2}^L}^2 = \left(\delta^L\right)^2 \sigma_{r_{q2}^L}^2 \tag{E.6}$$

$$\sigma_{r_{11}}^2 = \left(\frac{\partial r_{11}}{\partial r_{11}^L}\right)^2 \sigma_{r_{11}^L}^2 = \left(\delta^L\right)^2 \sigma_{r_{11}^L}^2 \tag{E.7}$$

$$\sigma_{r_{22}}^2 = \left(\frac{\partial r_{22}}{\partial r_{22}^L}\right)^2 \sigma_{r_{22}^L}^2 + \left(\frac{\partial r_{22}}{\partial r_{q2}^L}\right)^2 \sigma_{r_{q2}^L}^2 = \left(\delta^L\right)^2 \sigma_{r_{22}^L}^2 + \left(2\Delta_{vap}H_2\delta^L\right)^2 \sigma_{r_{q2}^L}^2 \tag{E.8}$$

$$\sigma_{r_{12}}^2 = \left(\frac{\partial r_{12}}{\partial r_{12}^L}\right)^2 \sigma_{r_{12}^L}^2 + \left(\frac{\partial r_{12}}{\partial r_{q2}^L}\right)^2 \sigma_{r_{q2}^L}^2 = \left(\delta^L\right)^2 \sigma_{r_{12}^L}^2 + \left(\Delta_{vap}H_1\right)^2 \sigma_{r_{q2}^L}^2 \tag{E.9}$$

The propagation of error from the ethane mole fraction to the resistivities and resistances in tray 2 - 4 with chosen film thicknesses is calculated and given in table E.1. The value used as the error in the mole fraction is the deviation of the sum of the mole fractions from 1. The error propagation is calculated with the values obtained after the iteration is finished, and it do not show the full impact on the system. It just shows that the mole fractions have a considerable impact on some of the variables. Even an error of 0.015 in tray 2, causes an error of 15.5 % on r_{12}. From equation 2.73 and equation 2.55 - 2.57 we see how errors in the resistances and resistivities will propagate directly to the fluxes and temperature and chemical potential profiles.

Table E.1: The propagation of error in the ethane mole fraction to resistivities and resistances in tray 2 - 4. The values are calculated using Gauss' law of error propagation, and using values for finished iterations. The error is given in percentage of the absolute values of the resistivities and resistances, with three digits that is the precision of the values used for the calculation.

Value	error tray 2 [%]	error tray 3 [%]	error tray 4 [%]
x_1^{LI}	$1.50 \cdot 10^{-2}$	$5.00 \cdot 10^{-2}$	$5.00 \cdot 10^{-2}$
r_{q2}^L	6.77	20.3	36.3
r_{11}^L	3.63	12.3	22.8
r_{22}^L	9.86	27.9	40.3
r_{12}^L	7.54	22.3	49.8
r_{q2}	$2.07 \cdot 10^{-2}$	$6.89 \cdot 10^{-2}$	$7.66 \cdot 10^{-2}$
r_{11}	1.19	3.72	6.78
r_{22}	$2.49 \cdot 10^{-1}$	$8.00 \cdot 10^{-1}$	1.35
r_{12}	15.5	53.4	36.7

Nomenclature

$(J_{am}^{L,TK})$	Column vector with Taylor and Krishna's liquid diffusion fluxes relative to average molar velocity	mol/m^{2}s
$(J_{am}^{V,TK})$	Column vector with Taylor and Krishna's vapor diffusion fluxes relative to average molar velocity	mol/m^{2}s
$[\Gamma^P]$	Matrix with thermodynamic factors for phase P	
$[k^L]$	Matrix with Taylor and Krishna's liquid mass transfer coefficients	m/s
$[k^V]$	Matrix with Taylor and Krishna's vapor mass transfer coefficients	m/s
$[R^P]$	Matrix with mass transfer resistances for phase P	s/m
α_T	Thermal diffusion factor	
$\bar{D}_{12}$	Maxwell-Stefan diffusivity	m^2/s
$\bar{D}_{12}^P$	Maxwell-Stefan diffusivity of component 1 in component 2 in phase P	m^2/s
$\bar{r}^P$	Resistance in phase P	
ΔP_{j-1}	Pressure drop from stage $j-1$ to stage j	Pa
ΔT	Temperature difference	K
Δx	Length difference	m
δ^P	Diffusion film thickness in phase P	m
δ_μ^P	Mass diffusion film thickness in phase P	m
δ_q^P	Thermal diffusion film thickness in phase P	m
δ_{ij}	Kronecker delta	
$\Delta_{vap}H_i$	Evaporation enthalpy of component i	J mol^{-1}
$\frac{dS^{irr,I}}{dt}$	Entropy production in interface	J/(K s)
$\frac{dS^{irr,L}}{dt}$	Entropy production in liquid diffusion film	J/(K s)
$\frac{dS^{irr,P}}{dt}$	Entropy production in phase P diffusion film	J/(K s)
$\frac{dS^{irr,V}}{dt}$	Entropy production in vapor diffusion film	J/(K s)
$\frac{dS^{irr}}{dt}$	Total entropy production	J/(K s)
Γ^P	Thermodynamic factor for two-component system in phase P	

Γ_i	Excess interface concentration	mol m^{-2}
λ^P	Thermal conductivity of phase P	J/(m^2s)
λ^V	Thermal conductivity in vapor	J/(m^2s)
λ_i^V	Thermal conductivity of component i in vapor	J/(m^2s)
$\mathcal{E}_j^L$	Energy loss due to evaporation	J/s
$\mathcal{E}_j^V$	Energy loss due to condensation	J/s
$\mathcal{N}_{ij}$	Molar rate of phase transposition of component i on stage j	mol/s
$\mathcal{N}_{ij}^L$	Molar rate of phase transposition from liquid of component i on stage j	mol/s
$\mathcal{N}_{ij}^V$	Molar rate of phase transposition from vapor of component i on stage j	mol/s
$\mathcal{N}_{t_j}^L$	Total mass transfer rate from liquid phase in stage j	mol/s
$\mathcal{N}_{t_j}^V$	Total mass transfer rate from vapor phase in stage j	mol/s
$\mathcal{N}_{tj}^L$	Molar rate of total phase transposition from liquid in phase j	mol/s
$\mathcal{N}_{tj}^V$	Molar rate of total phase transposition from vapor in phase j	mol/s
μ_i^L	Liquid chemical potential for component i	J/mol
μ_i^V	Vapor chemical potential for component i	J/mol
$\mu_i^{V,0}$	Standard chemical potential for component i	J/mol
μ_i^I	Interface chemical potential for component i	J/mol
$\mu_{T,i}$	Chemical potential for component i differentiated at constant T	J mol^{-1}
$\overline{H^L}_{ij}$	Partial molar enthalpy of component i in liquid for stage j	J/mol
$\overline{H^V}_{ij}$	Partial molar enthalpy of component i in vapor for stage j	J/mol
ϕ_i^P	Fugacity coefficient for component i in phase P	
σ	Local entropy production	J K^{-1} m^{-3} s^{-1}
σ^P	Local entropy production in phase P	J K^{-1} m^{-3} s^{-1}
σ_i	Condensation coefficient for comonent i	
σ_x	Error in quantity x	
E_{ij}^L	Energy balance equation for liquid on stage j	J/s
E_{ij}^V	Energy balance equation for vapor on stage j	J/s
M_{ij}^I	Mass balance equation for interface of component i on stage j	mol/s
M_{ij}^L	Mass balance equation for liquid phase of component i on stage j	mol/s
M_{ij}^V	Mass balance equation for vapor phase of component i on stage j	mol/s
S_j^{LI}	Summation equation for liquid for stage j at interface	
S_j^{VI}	Summation equation for vapor for stage j at interface	

a_j	Interfacial area in stage j	m^2
c	Number of components in the system	
c^L	Total concentration in liquid phase	mol/m^3
c^P	Total concentration in phase P	mol m^{-2}
c^V	Total concentration in vapor phase	mol/m^3
c^V	Total concentration in vapor phase	mol m^{-3}
c_i^V	Concentration of component i in vapor phase	mol m^{-3}
D_{ij}^P	Molar diffusivity of component i in component j in phase P	m^2/s
F_j^L	Total molar liquid feed flow to stage j	mol/s
F_j^V	Total molar vapor feed flow to stage j	mol/s
f_{ij}^L	Molar feed flow rate of component i to stage j in liquid phase	mol/s
f_{ij}^V	Molar feed flow rate of component i to stage j in vapor phase	mol/s
h^P	Heat transfer coefficient	$J/(m^2Ks)$
h_j^L	Heat transfer coefficient in liquid for stage j	W/m^2K
h_j^V	Heat transfer coefficient in vapor for stage j	W/m^2K
H_j^{Lb}	Molar enthalpy of liquid in tray j	J/mol
H_j^{LF}	Molar enthalpy of liquid feed to tray j	J/mol
H_j^{Vb}	Molar enthalpy of vapor in tray j	J/mol
H_j^{VF}	Molar enthalpy of vapor feed to tray j	J/mol
I	Identity matrix	
$J_q'^P$	Measurable heat flux of phase P	$J/(m^2s)$
$J_{i,am}^P$	Integrated interface diffusional flux of component i in phase P relative to average molar velocity	mol m^{-2} s^{-1}
J_t^P	Integrated interface mixture molar flux of phase P	mol m^{-2} s^{-1}
$J_i^{L,TK}$	Taylor and Krishna's molar flux in liquid phase for component i	mol m^{-2} s^{-1}
$J_i^{V,TK}$	Taylor and Krishna's molar flux in vapor phase for component i	mol m^{-2} s^{-1}
J_1	Mass flux 1	$J/(m^2s)$
J_2	Mass flux 2	$J/(m^2s)$
J_i	Diffusion flux of component i	$mol/(m^2s)$
J_i	General symbol for flux of i	mol m^{-2} s^{-1} or J m^{-2} s^{-1}
$J_q'^V$	Measurable vapor heat flux	$J/(m^2s)$
$J_q^{L,TK}$	Taylor and Krishna's total heat flux in liquid due to interphase transfer	J/(mol s)

$J_q^{V,TK}$	Taylor and Krishna's total heat flux in vapor due to interphase transfer	J/(mol s)
J_s^P	Entropy flux for phase P	J K^{-1} s^{-1}
$J_t^{L,TK}$	Taylor and Krishna's liquid mixture molar flux	mol m^{-2} s^{-1}
$J_t^{V,TK}$	Taylor and Krishna's vapor mixture molar flux	mol m^{-2} s^{-1}
$J_{i,am}^{L,TK}$	Taylor and Krishna's diffusional liquid flux of component i relative to average molar velocity	mol m^{-2} s^{-1}
$J_{i,am}^{V,TK}$	Taylor and Krishna's diffusional vapor flux of component i relative to average molar velocity	mol m^{-2} s^{-1}
K_{ij}	K-value for component i at stage j	
k_{ij}^P	Taylor and Krishna's binary mass transfer coefficients for phase P	
L_j	Molar flow rate in liquid phase from stage j	mol/s
L_{ij}, l_{ij}	Conductivity coefficient for coupling of fluxes i and j	
M_i	Molar mass	kg mol^{-1}
p	Total pressure if in vapor, vapor pressure if in liquid	Pa
p_i^*	Vapor pressure of component i	Pa
p_0	Standard pressure	Pa
P_c	Pressure of the condenser	Pa
P_j	Pressure of stage j	Pa
P_s	Specified pressure at the top tray	Pa
Q	Heat added or withdrawed from column	J/s
q_i*	Measurable heat of transfer for component i	J/mol
R	Gas constant	J K^{-1} mol^{-1}
R_{ij}, r_{ij}	Resistivity coefficient for coupling of fluxes i and j	
r_{ij}^P*	Resistivity found from Taylor and Krishna's equations	
s^P	Entropy density for phase P	J K^{-1} m^{-3}
T^{LI}	Temperature at liquid side of interface	K
T^{VI}	Temperature at vapor side of interface	K
T_j^I	Temperature in interface in stage j	K
T_j^{Lb}	Temperature in liquid bulk in stage j	K
T_j^{Vb}	Temperature in vapor bulk in stage j	K
u^P	Internal energy density for phase P	J m^{-3}
V_j	Molar flow rate in vapor phase from stage j	mol/s
v_{mp}	Average of most probable velocities	m/s

x_{ij}^{Lb}	Molar fraction of component i from stage j in liquid phase	
X_1^I	Driving force konjugate to mass flux 1 in interface	J mol^{-1} K^{-1} m^{-1}
X_1^L	Driving force konjugate to mass flux 1 in liquid	J mol^{-1} K^{-1} m^{-1}
X_1^P	Driving force konjugate to mass flux 1 in phase P	J mol^{-1} K^{-1} m^{-1}
X_1^V	Driving force konjugate to mass flux 1 in vapor	J mol^{-1} K^{-1} m^{-1}
$X_1^{P,loc}$	Local driving force konjugate to mass flux 1 in phase P	J mol^{-1} K^{-1} m^{-1}
X_2^I	Driving force konjugate to mass flux 2 in interface	J mol^{-1} K^{-1} m^{-1}
X_2^L	Driving force konjugate to mass flux 2 in liquid	J mol^{-1} K^{-1} m^{-1}
X_2^P	Driving force konjugate to mass flux 2 in phase P	J mol^{-1} K^{-1} m^{-1}
X_2^V	Driving force konjugate to mass flux 2 in vapor	J mol^{-1} K^{-1} m^{-1}
$X_2^{P,loc}$	Local driving force konjugate to mass flux 2 in phase P	J mol^{-1} K^{-1} m^{-1}
X_i	Driving force konjugate to flux i	J mol^{-1}m^{1}K^{-1} or K^{-1}m^{-1}
$X_q'^I$	Driving force konjugate to measurable heat flux at vapor side in interface	K^{-1}m^{-1}
$X_q'^L$	Driving force konjugate to measurable heat flux in liquid	K^{-1}m^{-1}
$X_q'^P$	Driving force konjugate to measurable heat flux in phase P	K^{-1}m^{-1}
$X_q'^V$	Driving force konjugate to measurable heat flux in vapor	K^{-1}m^{-1}
$X_q'^{P,loc}$	Local driving force konjugate to measurable heat flux in phase P	K^{-1}m^{-1}
x_{ij}^I	Liquid mole fraction of component i at stage j at interface	
y_{ij}^I	Vapor mole fraction of component i at stage j at interface	
y_{ij}^{Vb}	Molar fraction of component i from stage j in vapor phase	
z_i	Mole fraction of component i in arbitrary phase	
s_T	General Soret coeffcient	
s_T^L	Liquid Soret coeffcient	
s_T^V	Vapor Soret coeffcient	
v_i	Velocity of component i	mol/s

Bibliography

[1] ChemSep. Website, 2009. http://www.chemsep.org [accessed: 22. June 2009].

[2] D. Bedeaux and S. Kjelstrup. Irreversible thermodynamics - a tool to describe phase transitions far from global equilibrium. *Chemical Engineering Science*, 59:109–118, 2004.

[3] D. Bedeaux, J. Smith, L. Hermans, and T. Ytrehus. Slow evaporation and condensation ii. a dilute mixture. *Physica A*, 182:388 – 418, 1992.

[4] R. Bock and L. van der Ham. Personal communication. Institute of Chemistry, Norwegian University of Technology and Science, Norway, 2009.

[5] K. S. Førland, T. Førland, and S. Kjelstrup. *Irreversible Thermodynamics - Theory and Applications*. Tapir Academic Press, 1988.

[6] J. O. Hirscfelder, C. F. Curtiss, and R. B. Bird. *Molecular Theory of Gases and Liquids*. John Wiley & Sons, 1964.

[7] J. L. Humphrey and A. F. Siebert. Separation technologies: An opportunity for energy savings. *Chemical Engeneering Progress*, 88(3), 1992.

[8] L. J. T. M. Kempers. A thermodynamic theory of the soret effect in a multicomponent liquid. *Journal of Chemical Physics*, 90:6541–6548, 1989.

[9] C. J. King. *Separation Processes*. McGraw-Hill, 2 edition, 1980.

[10] S. Kjelstrup and D. Bedeaux. *Non-Equilibrium Thermodynamics of Heterogeneous Systems*. World Scientific, 2008.

[11] S. Kjelstrup and G. M. de Koeijer. Transport equations for distillation of ethanol and water from the entropy production rate. *Chemical Engineering Science*, 58:1147–1161, 2003.

[12] H. A. Kooijman and R. Taylor. *The ChemSep Book*. 2006.

[13] R. Krishna and J. A. Wesselingh. The maxwell-stefan approach to mass transfer. *Chemical Engineering Science*, 52:861–911, 1997.

[14] R. Krishnamurthy and R. Taylor. A nonequilibrium stage model of multicomponent separation processes:i-iii. *AIChE*, 1985.

[15] P. C. Mørk. *Overflate og koloidkjemi. Grunnleggende prinsipper og teorier.* NTNU, Institutt for kjemisk prosessteknologi, 8 edition, 2004.

[16] R. C. Reid, J. M. Prausnitz, and B. E. Poling. *The Properties of Gases and Liquids*. McGraw-Hill, 4 edition, 1986.

[17] R. Taylor and R. Krishna. *Multicomponent Mass Transfer*. John Wiley & sons, Inc., 1993.